Archive of Applied Mechanics (2022) 92:1997–2017
https://doi.org/10.1007/s00419-022-02173-7

REVIEW

Marko V. Lubarda · **Vlado A. Lubarda**

A review of the analysis of wind-influenced projectile motion in the presence of linear and nonlinear drag force

Received: 25 September 2021 / Accepted: 26 April 2022 / Published online: 23 May 2022

Abstract The analysis of wind-influenced projectile motion in the case of linear and nonlinear (quadratic or nonquadratic) drag force is reviewed. For quadratic or more general nonlinear drag force, the results can be obtained only numerically, because the governing coupled differential equations of motion do not allow an analytical solution, although there is a closed-form relationship between the velocity and an appropriately defined angle parameter in the case of quadratic drag. For linear drag force, the entire solution, including the expressions for the time-variation of velocity components and the shape of the trajectory, can be derived in closed form. Forward-to-backward transition of the direction of motion of a projectile launched against horizontal wind is analyzed. If during different phases of motion different types of drag apply, the extents of these phases are not known in advance and the general expression for the drag force that encompasses the entire range of the Reynolds number must be used throughout the motion, in conjunction with the numerical solution of the governing differential equations. The transition from nonquadratic to quadratic drag is discussed. Illustrative examples of wind-influenced projectile motion considered in this review include the motion of golf balls, respiratory droplets, powder particles, and flea beetles.

Keywords Linear drag · Nonlinear drag · Projectile motion · Quadratic drag · Reynolds number · Terminal velocity · Wind effect

1 Introduction

The study of projectile motion is of great importance for numerous areas of engineering and technology, including external ballistics for military applications, sports techniques and technologies, design of spreaders for distributing pelletized feed in aquacultural engineering, bio-ballistics with applications to agricultural engineering, metal sparks spreading during machine grinding in manufacturing engineering, powder technology, and inkjet printing technology. Fundamentally important in this analysis is the modelling of the drag force exerted by the surrounding medium on the flying object. The present paper offers a review of the analysis of projectile motion in the presence of linear and nonlinear (quadratic or nonquadratic) drag force. In the absence of wind, the magnitude of the drag force in the model of quadratic drag is proportional to the square of the velocity of the projectile, $F_{\rm d} = cv^2$, where c is the damping resistance coefficient [1–4]. For example, for a spherical ball of radius R moving in the air, $c = (1/2)c_{\rm d}\rho_{\rm air}A$, where $c_{\rm d} = 0.47$ is the experimentally determined aerodynamic drag coefficient, $\rho_{\rm air}$ is the air density, and $A = \pi R^2$ is the mid-cross-sectional

M. V. Lubarda (✉)
Department of Mechanical and Aerospace Engineering, UC San Diego, La Jolla, CA 92093-0411, USA
E-mail: mlubarda@ucsd.edu

V. A. Lubarda
Department of NanoEngineering, UC San Diego, La Jolla, CA 92093-0448, USA

area. This type of drag, known as quadratic (Newton's) drag, applies in the range of the Reynolds number, $10^3 < \mathrm{Re} = 2Rv/\nu_{\mathrm{air}} < 3 \times 10^5$, where ν_{air} is the kinematic viscosity of air. The quadratic drag model, with the appropriate value of c_{d} and the appropriate expression for the cross-sectional area A, applies to the motion of baseballs, golf balls, stones, arrows, cannonballs, and other mechanically shot projectiles [5–8].

The magnitude of the drag force in the model of linear damping is proportional to the velocity, $F_{\mathrm{d}} = c_{\mathrm{L}} v$, where, for a spherical projectile, $c_{\mathrm{L}} = 6\pi\eta_{\mathrm{air}} R$, with $\eta_{\mathrm{air}} = \nu_{\mathrm{air}}\rho_{\mathrm{air}}$ being the dynamic viscosity of air [9,10]. This type of drag is known as Stokes' drag, and it applies in the range of small Reynolds number ($\mathrm{Re} < 1$), i.e., for slow (creepy) flows. The linear damping model is of less importance for the study of common projectiles, where the velocities and sizes of the flying objects are too high for the adoption of the Stokes' flow assumption, but it is of interest and is often used in the study of sedimentation of pollutants or settlements of other very light and small particles (silt in water, mist in the atmosphere, microorganisms in water) [1,11]. It has also been used in the study of inkjet systems and the determination of the charged ink drop path [12], and in studying the motion of very small respiratory droplets, ejected by breathing or soft talking [13].

For the intermediate range of the Reynolds number ($1 < \mathrm{Re} < 1000$), the drag force is a more complicated nonlinear function of velocity. It is commonly specified as $F_{\mathrm{d}} = (1/2)c_{\mathrm{d}}\rho_{\mathrm{air}} A v^2$ [14,15], with the drag coefficient $c_{\mathrm{d}} = c_{\mathrm{d}}(\mathrm{Re})$ expressed in terms of the Reynolds number by fitting experimental data. Various expressions for the relationship $c_{\mathrm{d}} = c_{\mathrm{d}}(\mathrm{Re})$ have been listed in references [16,17]. For example, the expressions $c_{\mathrm{d}} = 24/\mathrm{Re} + 3/\mathrm{Re}^{0.28}$ and $c_{\mathrm{d}} = 21.12/\mathrm{Re} + 6.3/\sqrt{\mathrm{Re}} + 0.25$ have been used. Approximate expressions for the entire range of the Reynolds number up to 2×10^5 in the form $c_{\mathrm{d}} = 24/\mathrm{Re} + 6/(1 + \sqrt{\mathrm{Re}}) + 0.4$ and $c_{\mathrm{d}} = (0.63 + 4.8/\sqrt{\mathrm{Re}})^2$ have also been proposed. In the presence of wind whose velocity is $\boldsymbol{v}_{\mathrm{w}}$, the drag force is $\mathbf{F}_{\mathrm{d}} = -(1/2)c_{\mathrm{d}}\rho_{\mathrm{air}} A|\boldsymbol{v} - \boldsymbol{v}_{\mathrm{w}}|(\boldsymbol{v} - \boldsymbol{v}_{\mathrm{w}})$, where $c_{\mathrm{d}} = c_{\mathrm{d}}(\mathrm{Re})$ and the Reynolds number is defined by $\mathrm{Re} = 2R|\boldsymbol{v} - \boldsymbol{v}_{\mathrm{w}}|/\nu_{\mathrm{air}}$. The magnitude of the velocity of the projectile relative to the wind is denoted by $|\boldsymbol{v} - \boldsymbol{v}_{\mathrm{w}}|$.

There have been numerous publications devoted to the study of projectile motion in the presence of ambient drag, particularly in the context of military and sports applications. We summarize below some of the recent ones, which include both research and pedagogical contributions of interest for applied physics and engineering education. An analytical solution for the projectile velocity as a function of time in form of a ratio of two series expansions has been derived in the case of quadratic drag in [18]. An approximate solution to the equations of projectile motion under air resistance in the limit of short and long times has been derived in [19], and for low angle ballistics in [20]. Additional analytical approximations have also been considered [21–23]. The effect of the initial spin of a ball and the resulting lift force on the projectile motion of the ball has been studied in references [24–27]. External fluid flow- and wind-influenced projectile motions were the topics of references [18,28,29]. The bio-ballistics of small projectiles, with applications to insect jumps and plants' shooting of their seeds, have been considered in [30,31]. The use of the Lambert W function in the analysis of projectile motion with linear drag has been investigated by several researchers [32–34]. The use of Excel spreadsheets to simulate projectile motion with air resistance was reported in references [35,36], while historical remarks about projectile motion under ambient conditions can be found in [15,18,37–39]. Experimental results for sports balls as projectiles were reported in [15,40,41]. Approximate formulas for spherical projectiles of shotguns or muzzleloaders using nonlinear drag model with Mach dependent drag coefficient have been derived in [42]. Classical mechanics and physics textbooks also address various aspects of projectile motion [43–45]. Inelastic bouncing of a spherical ball in the presence of quadratic drag with application to sports balls has been studied in [46]. The models of linear and quadratic damping have also been used in the analysis of pendulums undergoing large swings, as recently reviewed in [47].

The contents of the present review are as follows. The analysis of projectile motion in the case of quadratic drag is presented in Sect. 2. The shape of the trajectory is depicted for any value of the damping parameter c and the specified initial velocity v_0 and ejection angle φ_0 by normalizing the spatial coordinates x and y with the length scale k^{-1}, where $k = c/m = g/v_{\mathrm{T}}^2$, with $v_{\mathrm{T}} = \sqrt{mg/c}$ being the terminal velocity at which the weight of the projectile (mg) is balanced by the drag force. The time scale used in the analysis is $\tau = v_{\mathrm{T}}/g$, where g is the gravitational acceleration. The trajectories are obtained numerically, because the governing equations of motion are coupled nonlinear ordinary differential equations, which do not allow a closed-form solution. For shallow trajectories (low angle ballistics), there is an approximate but sufficiently accurate analytical solution. In the absence of wind, the use of natural coordinates enable the derivation of a closed-form expression for the velocity $v = v(\varphi)$ in terms of the trajectory slope angle φ. With a modified angle parameter ϕ, the closed-form solution $v = v(\phi)$ also exists in the presence of uniform wind. The effects of wind on the projectile's trajectory and the flight velocity are evaluated and discussed. The analysis of projectile motion in the case of linear drag is presented in Sect. 3. The differential equations for the velocity components are in this case

decoupled, which greatly facilitates the analysis and allows for the derivation of closed-form expressions for the velocity components, trajectory and elapsed time during the motion, with or without the presence of wind. The corresponding damping coefficient is denoted by c_{L}, the parameter $k_{\mathrm{L}} = c_{\mathrm{L}}/m$ has the dimension of time^{-1}, and the terminal velocity is $v_{\mathrm{T,L}} = mg/c_{\mathrm{L}}$. The values of k_{L} are commonly so large that the trajectories of the projectiles in the range of linear drag (Re$<$ 1) dominantly consist of two nearly straight lines, on the time scale of a fraction of the second or longer. Because the horizontal momentum is rapidly reduced by drag to almost zero, the horizontal range of the projectile is much smaller than the horizontal range in the absence of drag. This is illustrated by the motion of small respiratory droplet and a tungsten powder particle. Forward-to-backward transition of the direction of motion in the case when the particle is ejected against the wind is also discussed. In Sect. 4, the projectile motion is considered in the range of the Reynolds number in which neither the linear nor quadratic drag model applies, but a more general nonlinear drag model in which the drag coefficient c_{d} is a nonlinear function of the Reynolds number. For some projectiles, the values of the Reynolds number can change during motion in such a way that during one phase of motion quadratic drag applies, while during another phase nonquadratic drag applies. Since the extents of different phases are not known in advance, for such projectiles it is necessary to use the general expression for the drag force which encompasses the entire range of the Reynolds number, and solve the corresponding equations of motion numerically. The transition from nonquadratic to quadratic drag is also discussed. Closing remarks are given in Sect. 5.

2 Projectile motion under quadratic drag

Figure 1a shows a spherical projectile of mass m launched from the ground or platform at $y = 0$ with the initial velocity v_0 at an angle φ_0 with respect to the horizontal x axis. If the air resistance is quadratic in the velocity v, the equations of motion in still air (without wind) are [15,18]

$$\frac{\mathrm{d}v_x}{\mathrm{d}t} = -kvv_x, \quad \frac{\mathrm{d}v_y}{\mathrm{d}t} = -kvv_y - g, \quad (k = c/m), \tag{2.1}$$

where $v_x = v\cos\varphi$ and $v_y = v\sin\varphi$ are the velocity components of the projectile, and $v = (v_x^2 + v_y^2)^{1/2}$. These equations follow by applying either Newton's or Lagrangian equations of motion. The parameter k has the dimension length^{-1}. The buoyancy force is not included in (2.1), which is satisfactory if the mass density of the projectile is much larger than the mass density of the surrounding air [3].

It is also assumed that the spin of the projectile is absent or ignored; its inclusion gives rise to the side or lift force, orthogonal to the drag force, as has been recently discussed in [24–26]. In the nondimensional form, (2.1) is

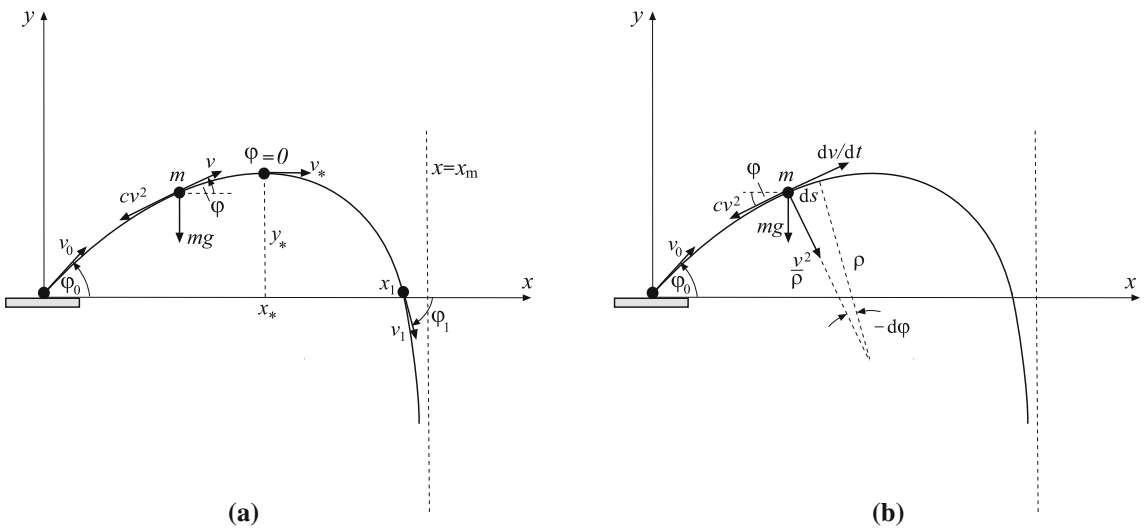

Fig. 1 **a** The motion of a spherical projectile of mass m launched from the ground with initial velocity v_0 at an angle φ_0 with respect to the horizontal x axis. At the flight position shown, the forces acting on the projectile are its weight mg and the drag force cv^2, opposite to its current velocity v. **b** The tangential and normal components of acceleration are $\mathrm{d}v/\mathrm{d}t$ and v^2/ρ, where ρ is the current radius of curvature of the trajectory. The infinitesimal arc-length of the trajectory is $\mathrm{d}s = -\rho\,\mathrm{d}\varphi$

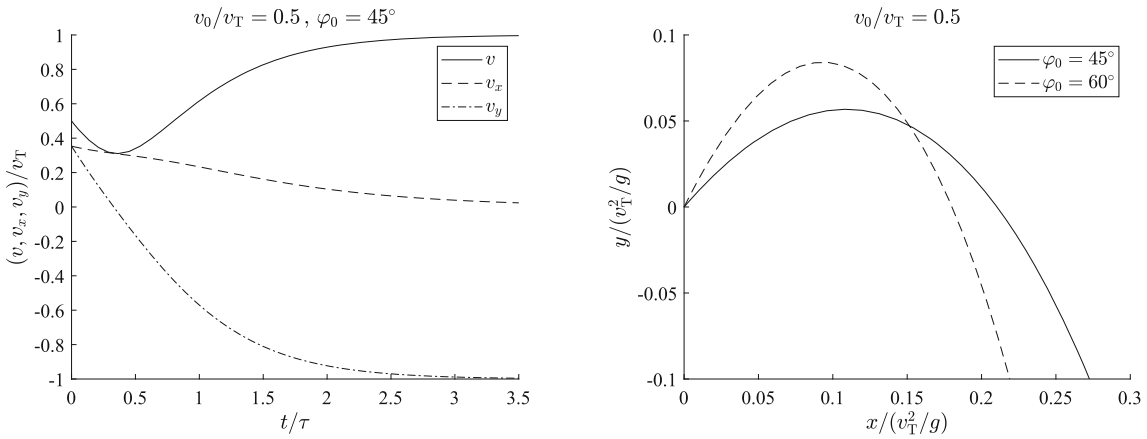

(a) **(b)**

Fig. 2 **a** The variation of the velocity components (v_x, v_y) and the total velocity $v = (v_x^2 + v_y^2)^{1/2}$ with the nondimensional time t/τ ($\tau = v_\mathrm{T}/g$) for the initial velocity $v_0 = 0.5v_\mathrm{T}$ and the launch angle $\varphi_0 = 45°$. Velocities are scaled by the terminal velocity v_T, and g is the acceleration of gravity. **b** The projectile trajectory $y = y(x)$ in the case of initial velocity $v_0 = 0.5v_\mathrm{T}$ and two values of the launch angle, $\varphi_0 = 45°$ and $\varphi_0 = 60°$. The normalizing length used in the plots is v_T^2/g

$$\frac{\mathrm{d}(v_x/v_\mathrm{T})}{\mathrm{d}(t/\tau)} = -(v_x/v_\mathrm{T})(v/v_\mathrm{T}), \quad \frac{\mathrm{d}(v_y/v_\mathrm{T})}{\mathrm{d}(t/\tau)} = -(v_y/v_\mathrm{T})(v/v_\mathrm{T}) - 1, \tag{2.2}$$

where $v_\mathrm{T} = (mg/c)^{1/2}$ is the terminal velocity and $\tau = v_\mathrm{T}/g$ is the time-parameter. The equations in (2.2) represent a system of two coupled first-order nonlinear ordinary differential equations for the velocity components $v_x = v_x(t)$ and $v_y = v_y(t)$, subject to the initial conditions $v_x(0) = v_0 \cos\varphi_0$ and $v_y(0) = v_0 \sin\varphi_0$. There is no closed-form solution to (2.2), but the equations can be solved readily by numerical means using, for example, the MATLAB function *ode45*, which implements a Runge–Kutta method with a variable time step for high accuracy and efficient computation. Figure 2a shows the variation of the nondimensional velocity components $(v_x, v_y)/v_\mathrm{T}$, and the magnitude of the velocity v/v_T, with the nondimensional time t/τ, for the launch angle $\varphi_0 = 45°$ and initial velocity $v_0 = v_\mathrm{T}/2$. In the limit as time increases indefinitely, the velocity v approaches the terminal velocity v_T, while $v_x \to 0$. Having the velocity components determined, the parametric equations of the trajectory $x = x(t)$ and $y = y(t)$ are obtained by numerical integration of $\mathrm{d}x/\mathrm{d}t = v_x(t)$ and $\mathrm{d}y/\mathrm{d}t = v_y(t)$ using the MATLAB function *cumtrapz*, which computes the cumulative integral by the trapezoidal method of integration. The corresponding plots are shown in Fig. 2b in the case $v_0 = v_\mathrm{T}/2$ and for the launch angles $\varphi_0 = 45°$ and 60°. The initial position of the projectile is $x_0 = y_0 = 0$.

Equations of motion (2.1) can be rewritten by eliminating the time increment $(\mathrm{d}t)$ in terms of the infinitesimal arc length $(\mathrm{d}s)$ using $v = \mathrm{d}s/\mathrm{d}t$ [1,18]. This gives

$$\frac{\mathrm{d}v_x}{\mathrm{d}s} = -kv_x, \quad \frac{\mathrm{d}v_y}{\mathrm{d}s} = -k\left(\frac{v_\mathrm{T}^2}{v} + v_y\right). \tag{2.3}$$

The solution to the first equation in (2.3) is $v_x(s) = v_x(0)\exp(-ks)$. Thus, $v_x \to 0$ as $s \to \infty$, which means that the trajectory has a vertical asymptote along which $v_y \to -v_\mathrm{T}$. Equation (2.3) also allows a simple analysis of the trajectory shape in the limiting cases of very small and very large launch velocity [15]. For example, if $v_0 \gg v_\mathrm{T}$, the initial portion of the trajectory is nearly a straight line $y = (\tan\varphi_0)x$. Furthermore, it follows that

$$\frac{\mathrm{d}^2y}{\mathrm{d}x^2} = \frac{\mathrm{d}}{\mathrm{d}x}\left(\frac{v_y}{v_x}\right) = \frac{1}{\cos\varphi}\left(\frac{1}{v_x}\frac{\mathrm{d}v_x}{\mathrm{d}s} - \frac{v_y}{v_x^2}\frac{\mathrm{d}v_x}{\mathrm{d}s}\right). \tag{2.4}$$

Thus, by substituting (2.3) into (2.4), one obtains

$$\frac{\mathrm{d}^2y}{\mathrm{d}x^2} = -\frac{g}{v_x^2}, \quad v_x = v_x(0)\exp(-ks). \tag{2.5}$$

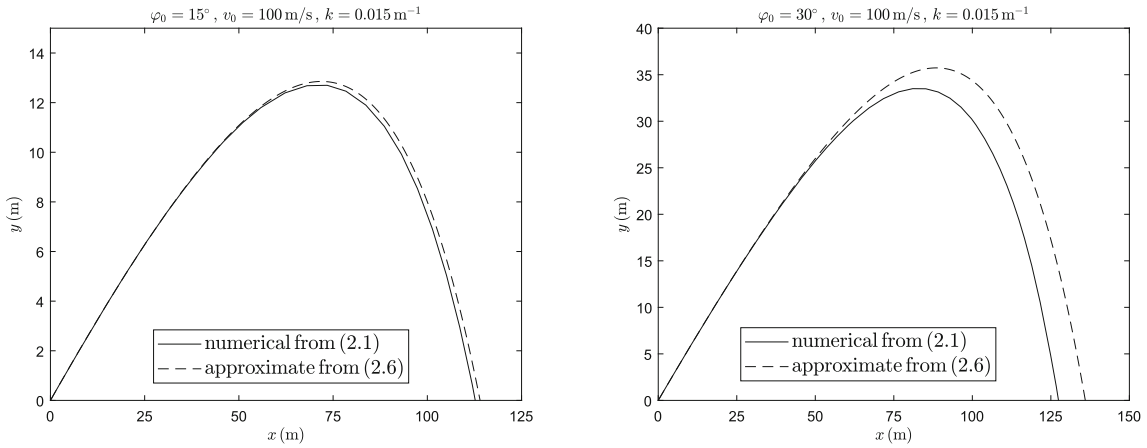

Fig. 3 **a** The trajectory of a spherical bullet of radius $R = 0.01$ m and mass $m = 0.006$ kg, fired with initial velocity $v_0 = 100$ m/s at an angle $\varphi_0 = 15°$. The trajectory obtained by numerical integration of equations (2.1) is shown by a solid line, and the trajectory obtained from the approximate expression (2.6) by a dashed line. **b** The predicted trajectories of the same bullet in the case $\varphi_0 = 30°$

An alternative derivation of (2.5), based on the expression for the curvature of the trajectory, has been given in [1]. Expression (2.5) can be integrated analytically to determine an approximate shape of a shallow projectile trajectory by replacing s with x. The result is

$$y = x\tan\varphi_0 - \frac{gx^2}{2v_0^2\cos^2\varphi_0^2}\,Z(x), \quad Z(x) = \frac{\exp(2kx) - 2kx - 1}{(2kx)^2/2}. \tag{2.6}$$

In the absence of drag, $Z(x) = 1$. For example, Fig. 3a shows the trajectory of a spherical bullet of radius $R = 0.01$ m and mass $m = 0.006$ kg, which is fired in stagnant air with initial velocity $v_0 = 100$ m/s at an angle $\varphi_0 = 15°$. The corresponding quadratic damping parameter is $k = c/m = 0.015\,\mathrm{m}^{-1}$. There is only a small difference between the shapes of the trajectories obtained by numerical integration of equations (2.1), and by using the approximate expression (2.6). The bullet will hit the ground at $x = 114$ m in the former case, and at $x = 115$ m in the latter case. If air resistance was ignored the bullet would hit the ground at $x = 509.7$ m. The difference between the shapes of the trajectories obtained from (2.1) and (2.6) is smaller for smaller angles $\varphi_0 < 15°$. For $\varphi_0 = 10°$, the maximum horizontal reach obtained from (2.1) is $x(y = 0) = 98.5$ m, while (2.6) predicts 99 m. The corresponding maximum heights are $y_{\max} = 6.906$ m and 6.930 m, which are within 0.35% of each other. Figure 3b, on the other hand, shows the predicted trajectories in the case $\varphi_0 = 30°$, demonstrating a significant departure of the approximate from the actual trajectory, except during the early (almost linear) stage of motion.

2.1 Velocity expression $v = v(\varphi)$

The use of the natural coordinates (ρ, φ), where ρ is the radius of the current curvature of the projectile trajectory and φ is the angle between the tangent to the trajectory and the positive x axis (Fig. 1b), results in certain mathematical simplifications and decoupling of the equations of motion, which enables the derivation of the closed-form expression for the velocity $v = v(\varphi)$ (Bernoulli's parametrization, [18]). The radius of curvature ρ is related to the infinitesimal arc length $\mathrm{d}s$ by $\mathrm{d}s = -\rho\,\mathrm{d}\varphi$, and the magnitude of the velocity is $v = \mathrm{d}s/\mathrm{d}t$. The equations of motion with respect to the natural coordinates [1,21] are

$$\frac{\mathrm{d}v}{\mathrm{d}t} = -kv^2 - g\sin\varphi, \quad \frac{v^2}{\rho} = g\cos\varphi. \tag{2.7}$$

By using $-\rho\,\mathrm{d}\varphi = \mathrm{d}s = v\,\mathrm{d}t$, the two equations in (2.7) can be combined to obtain the first-order quasi-linear differential equation for v^2,

$$\cos\varphi\,\frac{\mathrm{d}v^2}{\mathrm{d}\varphi} - \frac{2}{v_{\mathrm{T}}^2}v^4 - 2\sin\varphi\,v^2 = 0. \tag{2.8}$$

The differential equation (2.8) can be solved by first recalling that in the absence of air drag the velocity is $v = v_0 \cos\varphi_0/\cos\varphi$, which suggests the solution in the form $v^2 = w(\varphi)/\cos^2\varphi$. When this is substituted into (2.8), the differential equation for the auxiliary function $w = w(\varphi)$ is found to be

$$\frac{\mathrm{d}w}{w^2} = \frac{2}{v_{\mathrm{T}}^2}\frac{\mathrm{d}\varphi}{\cos^3\varphi}, \tag{2.9}$$

whose solution is

$$\frac{1}{w_0} - \frac{1}{w} = \frac{1}{v_{\mathrm{T}}^2}[f(\varphi) - f(\varphi_0)], \quad f(\varphi) = \frac{\sin\varphi}{\cos^2\varphi} + \ln\frac{1+\sin\varphi}{\cos\varphi}. \tag{2.10}$$

Thus, the final expression for the velocity $v = v(\varphi)$ is

$$v = \frac{v_0\cos\varphi_0}{\cos\varphi}\frac{1}{\sqrt{1 + (v_0/v_{\mathrm{T}})^2\cos^2\varphi_0[f(\varphi_0) - f(\varphi)]}}. \tag{2.11}$$

In contrast to the drag-free projectile motion, the velocity v is not a linear function of the initial velocity v_0. In the limit $\varphi \to -\pi/2$, the velocity $v(\varphi) \to v_{\mathrm{T}}$, which is the terminal downward velocity at which the weight of the projectile mg is balanced by the drag force cv_{T}^2. The velocity at the highest point of the trajectory is $v_* = v(\varphi = 0)$. The time dependence of the angle φ can be determined by numerical integration of $\mathrm{d}\varphi/\mathrm{d}t = -g\cos\varphi/v$, which follows by differentiating $\tan\varphi = v_y/v_x$. In the absence of air resistance, $v = v_0\cos\varphi_0/\cos\varphi$ and $\tan\varphi = \tan\varphi_0 - gt/(v_0\cos\varphi_0)$.

2.1.1 Classical derivation

An alternative derivation of the velocity expression $v = v(\varphi)$ was used in [1]. It proceeds from the first equation in (2.1) by eliminating the time increment as $\mathrm{d}t = -v\,\mathrm{d}\varphi/(g\cos\varphi)$. After dividing by $\cos^3\varphi$, this gives

$$\frac{\mathrm{d}(v\cos\varphi)}{(v\cos\varphi)^3} = \frac{1}{v_{\mathrm{T}}^2}\frac{\mathrm{d}\varphi}{\cos^3\varphi}. \tag{2.12}$$

Thus, upon integration,

$$\frac{1}{v_0^2\cos^2\varphi_0} - \frac{1}{v^2\cos^2\varphi} = \frac{1}{v_{\mathrm{T}}^2}[f(\varphi) - f(\varphi_0)], \tag{2.13}$$

in agreement with (2.11). It is noted that there is a sign error in eq. (p) on page 101 of [1], and consequently the plus sign in the denominator of their final expression for the velocity (74) should be a minus sign. It is also noted that the logarithmic term in the expression for the function $f(\varphi)$ in (2.10) can be cast in different equivalent forms, e.g.,

$$\ln\frac{1+\sin\varphi}{\cos\varphi} \equiv \frac{1}{2}\ln\frac{1+\sin\varphi}{1-\sin\varphi} \equiv \ln\left[\tan\left(\frac{\varphi}{2} + \frac{\pi}{4}\right)\right].$$

The first representation was used in [15], the second was used in [1], and the third in [21,22].

2.2 Parametric representation of trajectory in terms of angle φ

Once the velocity expression (2.11) for $v = v(\varphi)$ has been determined, the trajectory of the projectile can be deduced from its parametric representation $x = x(\varphi)$ and $y = y(\varphi)$, using angle φ as a monotonically decreasing parameter. The latter is obtained by numerical integration from $\mathrm{d}x = v_x\,\mathrm{d}t = (v\cos\varphi)\mathrm{d}t$ and $\mathrm{d}y = (\tan\varphi)\mathrm{d}x$, after the time increment $\mathrm{d}t$ has been eliminated in favor of the angle increment $\mathrm{d}\varphi$. This gives

$$x(\varphi) = \frac{1}{g}\int_{\varphi}^{\varphi_0} v^2\mathrm{d}\varphi, \quad y(\varphi) = \frac{1}{g}\int_{\varphi}^{\varphi_0} v^2\tan\varphi\,\mathrm{d}\varphi, \tag{2.14}$$

where the coordinate origin has been placed at the launching point of the projectile. The maximum height of the projectile and its x location (Fig. 1a) are determined from $y_* = y(\varphi = 0)$ and $x_* = x(\varphi = 0)$. The vertical

asymptote to the projectile trajectory is $x_{\rm m} = x(\varphi = -\pi/2)$, referred by some as the aerodynamic wall [15]. In the absence of drag, $x_m \to \infty$.

The angle $\varphi_1 < 0$ which corresponds to the position $y = 0$ during the descent of the projectile after the maximum reached height, and the corresponding value of $x_1 = x(\varphi_1)$, can be determined from

$$y(\varphi_1) = y_* + \frac{1}{g}\int_{\varphi_1}^{0} v^2 \tan\varphi \,\mathrm{d}\varphi = 0, \quad x_1 = \frac{1}{g}\int_{\varphi_1}^{\varphi_0} v^2 \mathrm{d}\varphi = x_* + \frac{1}{g}\int_{\varphi_1}^{0} v^2 \mathrm{d}\varphi. \tag{2.15}$$

The numerical evaluation of integrals can be performed by using the MATLAB function *integral*. The determination of the (optimal) launch angle φ_0 that, for a given v_0, maximizes the distance x_1, has been studied in [15,22,47]. The outcome of the analysis is that the optimal launch angle decreases below the no-drag optimal angle of $\varphi_0 = 45^\circ$ with the increase in drag and the increase in launch velocity v_0. Alternatively, one can determine the minimum required launch velocity and the corresponding launch angle to reach a given distance $x_1 = L$. In the absence of air resistance, the result is $v_0^{\min} = \sqrt{Lg/2}$ at $\varphi_0 = 45^\circ$. The corresponding time to reach this distance is $t_1 = 2\sqrt{L/g}$. Basketball players possibly tend to shoot the ball with the minimum velocity required to bridge the distance from their hands to the basket along a projectile path.

The time corresponding to the angle φ follows by numerical integration,

$$t(\varphi) = \frac{1}{g}\int_{\varphi}^{\varphi_0} \frac{v(\varphi)}{\cos\varphi}\,\mathrm{d}\varphi, \tag{2.16}$$

with $t = 0$ at $\varphi = \varphi_0$. The velocity versus the time plot $v = v(t)$ can then be readily generated from the parametric equations $t = t(\varphi)$ and $v = v(\varphi)$, the latter being specified by (2.11). The times to reach the maximum height (y_*), and the position $(x, y) = (x_1, 0)$, are $t_* = t(\varphi = 0)$ and $t_1 = t(\varphi = \varphi_1)$. In the absence of drag ($v_0/v_{\rm T} = 0$), the ascending and descending times are equal to each other, both being equal to v_0/g. In the presence of drag, the descending time $(t_1 - t_*)$ is greater than the ascending time (t_*) [48]. The time to reach the terminal velocity $v_{\rm T}$ is infinitely large, $t(\varphi \to -\pi/2) \to \infty$, although the value of v_x rapidly approaches zero, while $|v_y|$ rapidly approaches the terminal velocity $v_{\rm T}$.

In the absence of drag, the well-known explicit expressions for relations $x = x(\varphi)$ and $y = y(\varphi)$ are [[1], p. 98]

$$x(\varphi) = \frac{v_0^2\cos^2\varphi_0}{g}(\tan\varphi_0 - \tan\varphi), \quad y(\varphi) = \frac{v_0^2}{2g}\left(1 - \frac{\cos^2\varphi_0}{\cos^2\varphi}\right). \tag{2.17}$$

The distance x_1 corresponding to $y_1 = 0$ is $x_1 = (v_0^2/g)\sin 2\varphi_0$, and thus $x_1^{\max} = x_1(\varphi_0 = \pi/4) = v_0^2/g$ with the symmetry property $x_1(\pi/4 - \theta) = x_1(\pi/4 + \theta)$ for $0 \le \theta \le \pi/4$ (Halley's symmetry, in the absence of drag [9,10]).

2.3 Wind effects

In the presence of wind whose velocity vector $\boldsymbol{v}_{\rm w}$ has the components $v_{{\rm w},x}$ and $v_{{\rm w},y}$ in the vertical plane of the launch velocity vector $\boldsymbol{v}_0$, the drag force in the model of quadratic damping is

$$\mathbf{F}_{\rm d} = -c|\boldsymbol{v} - \boldsymbol{v}_{\rm w}|(\boldsymbol{v} - \boldsymbol{v}_{\rm w}), \quad c = \frac{1}{2}c_{\rm d}\rho_{\rm air}(\pi R^2), \tag{2.18}$$

where the drag coefficient $c_{\rm d} = 0.47$ for the Reynolds number $\mathrm{Re} = 2R|\boldsymbol{v} - \boldsymbol{v}_{\rm w}|/\nu_{\rm air}$ in the range $10^3 \le \mathrm{Re} \le 3 \times 10^5$. Thus, the relative velocity $(\boldsymbol{v} - \boldsymbol{v}_{\rm w})$ appears in the definition of the Reynolds number and the drag force. The governing differential equations for the horizontal and vertical components of velocity are then, e.g., [18],

$$\begin{aligned} \frac{\mathrm{d}v_x}{\mathrm{d}t} &= -k[(v_x - v_{{\rm w},x})^2 + (v_y - v_{{\rm w},y})^2]^{1/2}(v_x - v_{{\rm w},x}), \\ \frac{\mathrm{d}v_y}{\mathrm{d}t} &= -k[(v_x - v_{{\rm w},x})^2 + (v_y - v_{{\rm w},y})^2]^{1/2}(v_y - v_{{\rm w},y}) - g, \end{aligned} \tag{2.19}$$

with initial conditions $v_x(0) = v_0\cos\varphi_0$ and $v_y(0) = v_0\sin\varphi_0$. Equations (2.19) are two coupled differential equations, which require numerical integration. After the velocity components v_x and v_y have been determined,

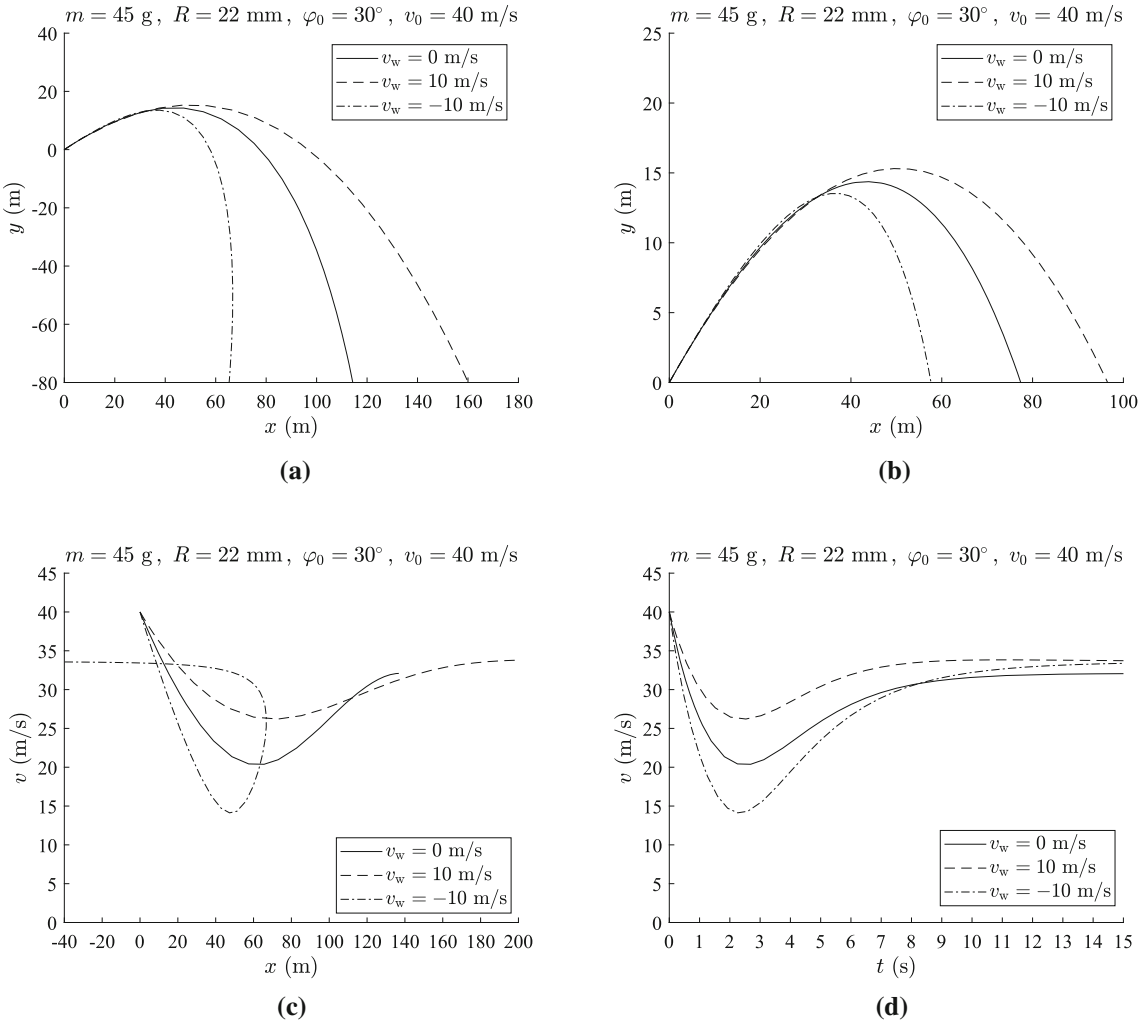

Fig. 4 **a** Trajectory of the ball of mass $m = 45$ g and radius $R = 45$ mm ejected with initial velocity $v_0 = 40$ m/s at an angle $\varphi_0 = 30°$. The three curves correspond to stagnant air (solid line), forward wind (dashed line), and backward wind (dash-dotted line), both with the wind speed of magnitude 10 m/s. **b** Portions of the plots from part **a** corresponding to $y \geq 0$. **c** Variations of the magnitude of the velocity v with the horizontal position x, and **d** the time t

the (x, y) coordinates of the trajectory follow by numerical quadrature from the velocity components, with initial conditions $x(0) = y(0) = 0$.

Motion of a golf ball Figure 4a shows the trajectory of the ball of mass $m = 45$ g and radius $R = 22$ mm ejected with initial velocity $v_0 = 40$ m/s at an angle $\varphi_0 = 30°$. The solid line curve is for the motion of the ball in stagnant air, the dashed line curve is for the motion in the presence of horizontal forward wind of magnitude 10 m/s, and the dash-dotted line curve is for the motion in the presence of the opposite direction of wind. In the absence of wind, the trajectory has a vertical asymptote $x = 136.78$ m, while the asymptotes in the case of forward and backward wind are tangent to the terminal velocity vector, whose slope is defined by the ratio $-v_\mathrm{T}/v_\mathrm{w} = \mp 3.14$, where $v_\mathrm{T} = (mg/c)^{1/2} = 32.09$ m/s is the magnitude of the vertical component of terminal velocity. Figure 4b shows the effect of wind on the maximum height of the ball and its maximum horizontal reach, in the case when the ground is at $y = 0$. In the absence of wind, as the ball approaches the vertical asymptote, the horizontal component of velocity $v_x \to 0$. In the presence of wind, the horizontal component of velocity approaches the speed of the wind $v_x \to v_\mathrm{w} = \pm 10$ m/s, while the vertical component of velocity approaches the vertical component of terminal velocity $v_y \to -v_\mathrm{T} = -32.09$ m/s. Parts (c) and (d) of Fig. 4 show the variations of the magnitude of the velocity $v = (v_x^2 + v_y^2)^{1/2}$ with respect to the horizontal position x and time t. The solid curve in Fig. 4c ends at $x = 136.78$ m, because, in the absence of wind, there is a vertical asymptote of the trajectory $x \to x_\mathrm{m} = 136.78$ m and in that limit $v \to v_\mathrm{T}$. In all three considered cases,

the motion of the ball is the range of the Reynolds number $4.81 \times 10^4 < \mathrm{Re} < 1.42 \times 10^5$, which validates the adopted quadratic drag assumption with the drag coefficient $c_\mathrm{d} = 0.47$. On the other hand, if the ball had a roughness of a golf ball, the transition from laminar to turbulent boundary layer, with the corresponding sudden drop of the drag coefficient, would take place at the Reynolds number of about 4×10^4 [49], which would require the use of the drag coefficient as law as 0.25 in the flow regime $\mathrm{Re} > 4 \times 10^4$.

2.4 Parametric expressions for velocity components in the presence of wind

By introducing the relative velocity $\boldsymbol{u} = \boldsymbol{v} - \boldsymbol{v}_\mathrm{w}$, equations of motion (2.19) can be written, in the case of constant wind velocity, as

$$\frac{\mathrm{d}u_x}{\mathrm{d}t} = -kuu_x, \quad \frac{\mathrm{d}u_y}{\mathrm{d}t} = -kuu_y - g, \tag{2.20}$$

where $u = (u_x^2 + u_y^2)^{1/2}$ is the magnitude of the relative velocity, and the initial conditions are $u_x(0) = v_x(0) - v_{\mathrm{w},x}$ and $u_y(0) = v_y(0) - v_{\mathrm{w},y}$. Equations in (2.20) are of the same form as equations in (2.1), and we can recognize from (2.8) that u^2 satisfies the first-order quasi-linear differential equation,

$$\cos\phi \frac{\mathrm{d}u^2}{\mathrm{d}\phi} - \frac{2}{v_\mathrm{T}^2}u^4 - 2\sin\phi\, u^2 = 0, \quad v_\mathrm{T}^2 = g/k. \tag{2.21}$$

The angle parameter ϕ is the angle between the relative velocity vector $\boldsymbol{u}$ and the positive x axis and is defined by [18]

$$\tan\phi = \frac{u_y}{u_x}. \tag{2.22}$$

In the absence of wind, the angle ϕ reduces to $\varphi = \tan^{-1}(v_y/v_x)$, which was used in Sect. 2.1. The solution to differential equation (2.21) is, from (2.11),

$$u = \frac{u_0\cos\phi_0}{\cos\phi}\frac{1}{\sqrt{1 + (u_0/v_\mathrm{T})^2\cos^2\phi_0[f(\phi_0) - f(\phi)]}}, \tag{2.23}$$

where $u_0^2 = u_x^2(0) + u_y^2(0)$, $\tan\phi_0 = u_y(0)/u_x(0)$, and the function f is as defined in (2.10).

Having determined the magnitude of the relative velocity $u = u(\phi)$, the relative velocity components follow from $u_x = u\cos\phi$ and $u_y = u\sin\phi$, while the components of the projectile velocity are $v_x = u_x + v_{\mathrm{w},x}$ and $v_y = u_y + v_{\mathrm{w},y}$. The relationship between the time t and the angle parameter ϕ is, in analogy with (2.16),

$$t(\phi) = \frac{1}{g}\int_\phi^{\phi_0} \frac{u(\phi)}{\cos\phi}\,\mathrm{d}\phi, \tag{2.24}$$

with $t = 0$ at $\phi = \phi_0$. Additional insightful aspects of the analysis can be found in [18].

3 Projectile motion under linear drag

The linear drag model is of less importance for the study of usual projectile motions, because the velocities and size of the launched projectiles are too large for the Stokes' drag assumption to apply. However, it may be of importance for the analysis of slow motion of very small particles, such as small respiratory droplets produced by soft talking and low ejection velocities [13]. We summarize below the main results of the analysis in the case when the drag force is linear in velocity $F_\mathrm{d} = c_\mathrm{L}v$, where c_L is the constant damping coefficient, as discussed in Sect. 1. The results can be given entirely in closed-form, which is a consequence of the fact that the corresponding governing equations for the velocity components v_x and v_y are decoupled,

$$\frac{\mathrm{d}v_x}{\mathrm{d}t} = -k_\mathrm{L}v_x, \quad \frac{\mathrm{d}v_y}{\mathrm{d}t} = -k_\mathrm{L}v_y - g, \quad (k_\mathrm{L} = c_\mathrm{L}/m), \tag{3.1}$$

and can be solved analytically to obtain [9,10,32]

$$v_x = v_0\cos\varphi_0\, e^{-k_\mathrm{L}t}, \quad v_y = v_{\mathrm{T,L}}\left(pe^{-k_\mathrm{L}t} - 1\right), \quad (v_{\mathrm{T,L}} = g/k_\mathrm{L} = mg/c_\mathrm{L}). \tag{3.2}$$

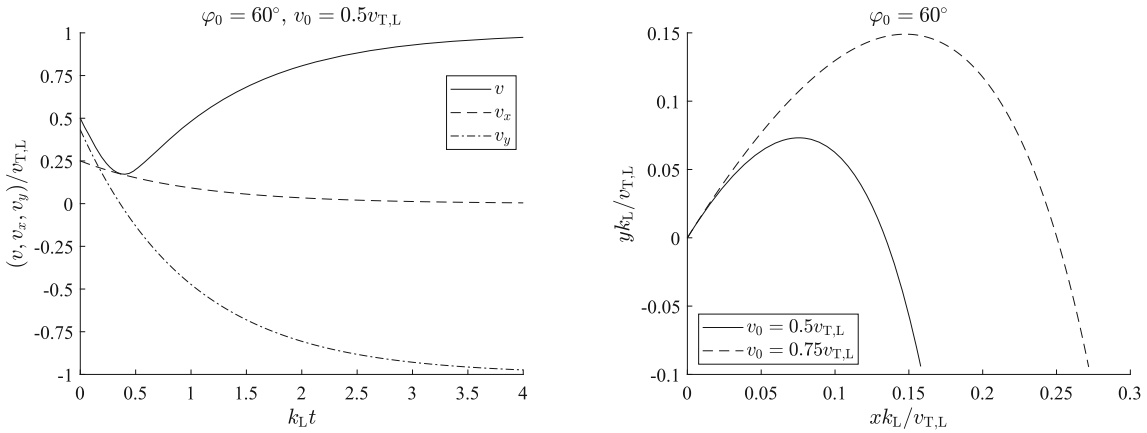

Fig. 5 **a** Variations of the velocity components (v_x, v_y) and the total velocity $v = (v_x^2 + v_y^2)^{1/2}$ with nondimensional time $k_{\mathrm{L}}t$ for the launch angle $\varphi_0 = 60°$ and the initial velocity $v_0 = 0.5v_{\mathrm{T,L}}$, according to the linear drag model. **b** The trajectory of the projectile in the case of two different launch velocities v_0, both at $\varphi_0 = 60°$. The lengths are scaled by $v_{\mathrm{T,L}}/k_{\mathrm{L}}$, where $v_{\mathrm{T,L}}$ is the corresponding terminal velocity

The nondimensional parameter p is defined by

$$p = 1 + \frac{v_0}{v_{\mathrm{T,L}}} \sin\varphi_0, \tag{3.3}$$

where $v_{\mathrm{T,L}}$ is the terminal velocity in the model of linear drag. The variations of the velocity components and the total velocity (scaled by $v_{\mathrm{T,L}}$) in the case of the initial velocity $v_0 = 0.5v_{\mathrm{T,L}}$ and the launch angle $\varphi_0 = 60°$ are shown in Fig. 5a.

Furthermore, by integration of $\mathrm{d}x = v_x\,\mathrm{d}t$ and $\mathrm{d}y = v_y\,\mathrm{d}t$, it follows that the parametric equations of the trajectory are

$$x = \frac{v_0}{k_{\mathrm{L}}} \cos\varphi_0 \left(1 - e^{-k_{\mathrm{L}}t}\right), \quad y = \frac{v_{\mathrm{T,L}}}{k_{\mathrm{L}}} \left[p\left(1 - e^{-k_{\mathrm{L}}t}\right) - k_{\mathrm{L}}t\right], \tag{3.4}$$

with time t as a monotonically increasing parameter. By eliminating $k_{\mathrm{L}}t$ in (3.4), the $y = y(x)$ representation of the trajectory is

$$y = \left(\tan\varphi_0 + \frac{v_{\mathrm{T,L}}}{v_0 \cos\varphi_0}\right) x + \frac{v_{\mathrm{T,L}}}{k_{\mathrm{L}}} \ln\left(1 - \frac{k_{\mathrm{L}}x}{v_0 \cos\varphi_0}\right). \tag{3.5}$$

The vertical asymptote to the trajectory is $x_{\mathrm{m}} = v_0 \cos\varphi_0/k_{\mathrm{L}}$, which follows from (3.4) in the limit $t \to \infty$. The trajectories of the projectile in the case of the launch velocities $v_0 = 0.5v_{\mathrm{T,L}}$ and $v_0 = 0.75v_{\mathrm{T,L}}$, and the launch angle $\varphi_0 = 60°$, are shown in Fig. 5b. The corresponding positions of the vertical asymptote are $x_{\mathrm{m}}k_{\mathrm{L}}/v_{\mathrm{T,L}} = 1/4$ and $3/8$. It is noted that the values of k_{L} are large in the case of linear drag and that the trajectories rapidly approach their vertical asymptotes. The very early portion of the trajectory is a straight line $y = (\tan\varphi_0)x$.

Motion of a respiratory droplet For a respiratory droplet of diameter 15 μm and mass $m = 1.762$ ng, ejected in stagnant air with velocity 1 m/s, the damping parameter is $c_{\mathrm{L}} = 2.58\,\mu$g/s; thus $k_{\mathrm{L}} = 1,464\,\mathrm{s}^{-1}$. The corresponding trajectories for three ejection angles are shown in Fig. 6a. For the most part, they consist of two nearly straight lines. The Reynolds number at the instant of ejection is Re=0.989, which rapidly decreases with subsequent rapid decrease of the droplet's velocity due to air drag. The corresponding variation of the velocity and its components with time in the case $\varphi_0 = 30°$ is shown in Fig. 6b. The terminal velocity is $v_{\mathrm{T,L}} = mg/c_{\mathrm{L}} = 6.7$ mm/s. In the absence of drag, $v_x = v_0 \cos\varphi_0 = $ const. and $v_y = v_0 \sin\varphi_0 - gt$, independently of R and m, while $x(y = 0) = (v_0^2/g) \sin 2\varphi_0$ =88.3 mm, about 150 times greater than $x_m = 0.59$ mm in the presence of linear drag.

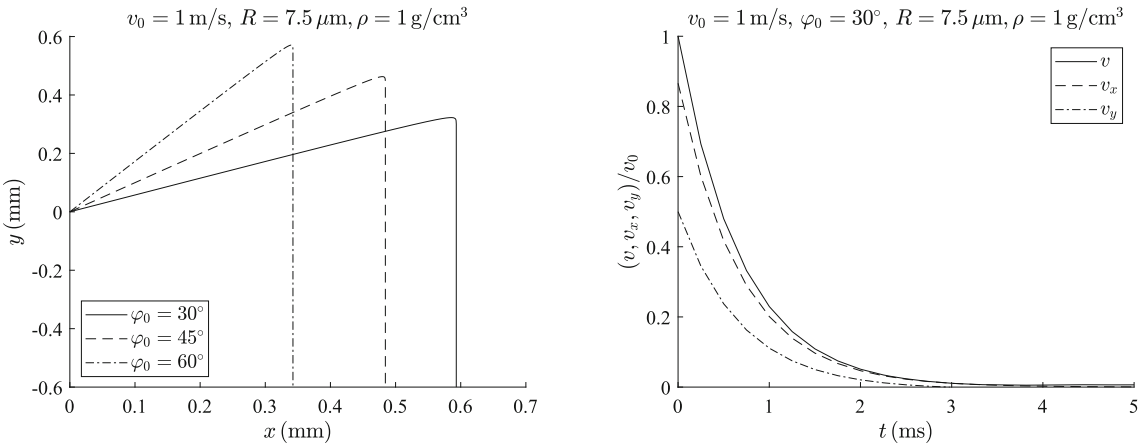

Fig. 6 **a** Trajectories of a respiratory droplet for three ejection angles in the case of linear drag. Vertical asymptotes are defined by $x_\mathrm{m} = v_0 \cos\varphi_0 / k_\mathrm{L}$. **b** Variations of the velocity v and its components (v_x, v_y) with time t for the launch angle $\varphi_0 = 30^\circ$ and the initial velocity $v_0 = 1$ m/s. While v_x rapidly approaches zero, $v_y \to v_{\mathrm{T,L}} = 6.7$ mm/s

3.1 Horizontal reach

The time $t_* = (1/k_\mathrm{L}) \ln p$ to reach the apex of the trajectory is obtained from the condition $v_y(t_*) = 0$. The corresponding (x_*, y_*) coordinates are

$$x_* = \frac{v_0^2}{2gp} \sin 2\varphi_0, \quad y_* = \frac{v_{\mathrm{T,L}}}{k_\mathrm{L}} (p - \ln p - 1). \tag{3.6}$$

If $0 < \varphi_0 < \pi/2$, the time t_1 to reach the point $(x_1, 0)$ is obtained by solving the equation $y(t_1) = 0$, i.e.,

$$p \left(1 - e^{-k_\mathrm{L} t_1}\right) - k_\mathrm{L} t_1 = 0, \tag{3.7}$$

which follows from the second expression in (3.4). Expressed in terms of the Lambert W function, the solution to (3.7) for $k_\mathrm{L} t_1$ is

$$k_\mathrm{L} t_1 = p + W\left(-p e^{-p}\right). \tag{3.8}$$

The corresponding coordinate x_1 (horizontal reach of the projectile) is then obtained by substituting (3.8) into the first expression in (3.4),

$$x_1 = \frac{v_0 \cos\varphi_0}{k_\mathrm{L}} \left[1 + \frac{1}{p} W\left(-p e^{-p}\right)\right]. \tag{3.9}$$

In the derivation, the definition of the Lambert W function $W(z) e^{W(z)} = z$ has been used [50,51]. Note that (3.9) also follows directly from equation (3.5) by solving it for x when $y = 0$. An expression for the optimum launch angle which maximizes the horizontal reach of the projectile, also given in terms of Lambert W function, has been derived and discussed in [10,33]. The corresponding analysis in the case when the launching point is higher than the landing point can be found in [34].

3.2 Velocity expression $v = v(\varphi)$

Similarly to the case of quadratic drag, a closed-form relationship $v = v(\varphi)$ can be derived in the case of linear drag. The governing differential equation for the velocity v in terms of the angle $\varphi = \tan^{-1}(v_y/v_x)$ can be cast in the form

$$\cos\varphi \frac{\mathrm{d}v}{\mathrm{d}\varphi} = \frac{1}{v_{\mathrm{T,L}}} v^2 + v \sin\varphi. \tag{3.10}$$

This equation can be solved by introducing an auxiliary function $w = w(\varphi)$, related to v by $v = w/\cos\varphi$, which transforms (3.10) into

$$\frac{\mathrm{d}w}{w^2} = \frac{1}{v_{\mathrm{T,L}}}\frac{\mathrm{d}\varphi}{\cos^2\varphi}. \tag{3.11}$$

Equation (3.11) can also be derived from eq. (64) of reference [1], p.97, which is valid for an arbitrary nonlinear drag, by taking $f(v) = 1$ in that equation and by making the substitution $w = v\cos\varphi$.

Upon integration of (3.11), the velocity is found to be

$$v = v_{\mathrm{T,L}}\left[\left(\tan\varphi_0 + \frac{v_{\mathrm{T,L}}}{v_0\cos\varphi_0}\right)\cos\varphi - \sin\varphi\right]^{-1}. \tag{3.12}$$

The velocity at the apex of the trajectory ($\varphi = 0$) is $v_* = (v_0/p)\cos\varphi_0$. If $c_{\mathrm{L}} \to 0$, the terminal velocity $v_{\mathrm{T,L}} \to \infty$, and (3.12) reduces to the well-known expression for the drag-free projectile motion [1], p.98, $v = v_0\cos\varphi_0/\cos\varphi$, while $v_* = v_0\cos\varphi_0$ (because $p = 1$).

3.3 Wind effects

In the presence of wind, the drag force is $\mathbf{F}_{\mathrm{d}} = -c_{\mathrm{L}}(\boldsymbol{v} - \boldsymbol{v}_{\mathrm{w}})$ and the governing equations for the velocity components become [6]

$$\frac{\mathrm{d}v_x}{\mathrm{d}t} = -k_{\mathrm{L}}(v_x - v_{\mathrm{w},x}), \quad \frac{\mathrm{d}v_y}{\mathrm{d}t} = -k_{\mathrm{L}}(v_y - v_{\mathrm{w},y}) - g. \tag{3.13}$$

These can be solved analytically to obtain [28,29]

$$v_x = v_{\mathrm{w},x}\left(1 - q_x e^{-k_{\mathrm{L}}t}\right) \quad v_y = (v_{\mathrm{w},y} - v_{\mathrm{T,L}})\left(1 - q_y e^{-k_{\mathrm{L}}t}\right), \tag{3.14}$$

where

$$q_x = 1 - \frac{v_0\cos\varphi_0}{v_{\mathrm{w},x}}, \quad q_y = 1 - \frac{v_0\sin\varphi_0}{v_{\mathrm{w},y} - v_{\mathrm{T,L}}}. \tag{3.15}$$

The parametric equations of the corresponding trajectory are then

$$x = \frac{v_{\mathrm{w},x}}{k_{\mathrm{L}}}\left[k_{\mathrm{L}}t - q_x\left(1 - e^{-k_{\mathrm{L}}t}\right)\right], \quad y = \frac{v_{\mathrm{w},y} - v_{\mathrm{T,L}}}{k_{\mathrm{L}}}\left[k_{\mathrm{L}}t - q_y\left(1 - e^{-k_{\mathrm{L}}t}\right)\right]. \tag{3.16}$$

If the wind is horizontal ($v_{\mathrm{w},x} = v_{\mathrm{w}}$, $v_{\mathrm{w},y} = 0$), the parameters in (3.15) reduce to

$$q_x = q = 1 - \frac{v_0\cos\varphi_0}{v_{\mathrm{w}}}, \quad q_y = p = 1 + \frac{v_0\sin\varphi_0}{v_{\mathrm{T,L}}}, \tag{3.17}$$

and the expressions for $v_y(t)$ and $y(t)$ in (3.14) and (3.16) become independent of the presence of wind. Thus, the time to reach the point $(x_1, y_1 = 0)$ is given by (3.8), provided that $0 < \varphi_0 < \pi/2$. The corresponding coordinate x_1 is obtained by substituting (3.8) into the first expression in (3.16),

$$x_1 = x(t_1) = \frac{v_{\mathrm{w}}\sin\varphi_0 + v_{\mathrm{T,L}}\cos\varphi_0}{v_0\sin\varphi_0 + v_{\mathrm{T,L}}}\,v_0 t_1. \tag{3.18}$$

On the other hand, in the case of backward wind ($v_{\mathrm{w}} < 0$), the time to reach the point $(x_2 = 0, y_2)$ is given by $k_{\mathrm{L}}t_2 = q + W\left(-qe^{-q}\right)$, which follows from (3.16). The corresponding coordinate y_2, obtained from the second expression in (3.16), can be expressed as

$$y_2 = y(t_2) = -\frac{v_{\mathrm{w}}\sin\varphi_0 + v_{\mathrm{T,L}}\cos\varphi_0}{v_0\cos\varphi_0 - v_{\mathrm{w}}}\,v_0 t_2, \quad v_{\mathrm{w}} < 0. \tag{3.19}$$

3.4 Forward-to-backward transition of motion

If the projectile is launched against horizontal wind ($v_{\mathrm{w}} < 0$) at an angle $0 < \varphi_0 < \pi/2$, it will eventually reverse its direction from the forward motion against the wind to the backward motion down the wind. The transition may take place by either upward or downward reversal of the direction of motion. The physical criterion for this transition is based on the comparison of the times to reach the points of the trajectory at which the horizontal and vertical components of the velocity are equal to zero,

$$t_{v_x=0} \begin{cases} < t_{v_y=0}, & \text{upward reversal,} \\ > t_{v_y=0}, & \text{downward reversal.} \end{cases} \tag{3.20}$$

The expressions for the times $t_{v_x=0}$ and $t_{v_y=0}$ are easily obtained from (3.14) and are given by $t_{v_x=0} = (1/k_{\mathrm{L}}) \ln q$ and $t_{v_y=0} = (1/k_{\mathrm{L}}) \ln p$. By substituting them into (3.20), it follows that the upward reversal occurs if $q < p$ and the downward reversal if $q > p$. Thus, in view of expressions (3.3) and (3.17) for p and q, the transition criterion is

$$|v_{\mathrm{w}}| \tan \varphi_0 \begin{cases} > v_{\mathrm{T,L}}, & \text{upward reversal,} \\ < v_{\mathrm{T,L}}, & \text{downward reversal.} \end{cases} \tag{3.21}$$

If the wind velocity and the angle of launch are related by $|v_{\mathrm{w}}| \tan \varphi_0 = v_{\mathrm{T,L}}$, the projectile moves along the straight line $y = (\tan \varphi_0)x$ up to the point with coordinates $x_* = x(t_*)$ and $y_* = y(t_*)$ at which both components of velocity are zero $v_x(t_*) = v_y(t_*) = 0$, where $t_* = (1/k_{\mathrm{L}}) \ln p$. The projectile then moves back along the same straight line. Indeed, if $|v_{\mathrm{w}}| \tan \varphi_0 = v_{\mathrm{T,L}}$ is substituted into the first expression in (3.14), it follows that $v_x = (\cot \varphi_0) v_y$, and therefore $y = (\tan \varphi_0)x$. The condition $|v_{\mathrm{w}}| \tan \varphi_0 = v_{\mathrm{T,L}}$ also follows by requiring that $x_1 = 0$ in (3.18), which was used in [28], where other inplane directions of wind were also considered. If the projectile is launched against the horizontal wind at an angle $-\pi/2 \le \varphi_0 \le 0$, the reversal of the direction of motion is necessarily downward, because v_y is always negative. The downward reversal of the direction of motion takes place when $v_x = 0$, i.e., at time $t = (1/k_{\mathrm{L}}) \ln q$.

Motion of a tungsten powder particle Figure 7a shows the early time trajectories (within a fraction of 1 s) of a tungsten powder particle of diameter 25 μm ejected at $\varphi_0 = 45°$ with initial velocity $v_0 = 50$ cm/s against a horizontal air stream with different velocity v_{w}, as indicated in the figure legend. The mass density of tungsten is taken to be 19 g/cm^3, thus $k_{\mathrm{L}} = 27.7\ \mathrm{s}^{-1}$ and $v_{\mathrm{T,L}} = 35.5$ cm/s. (The value of k_{L} for the tungsten particle is much smaller than the value of k_{L} for the previously considered respiratory droplet, because the mass density of tungsten is about 19 times greater than the density of water.) For $|v_{\mathrm{w}}| = v_{\mathrm{T,L}}$ the particle

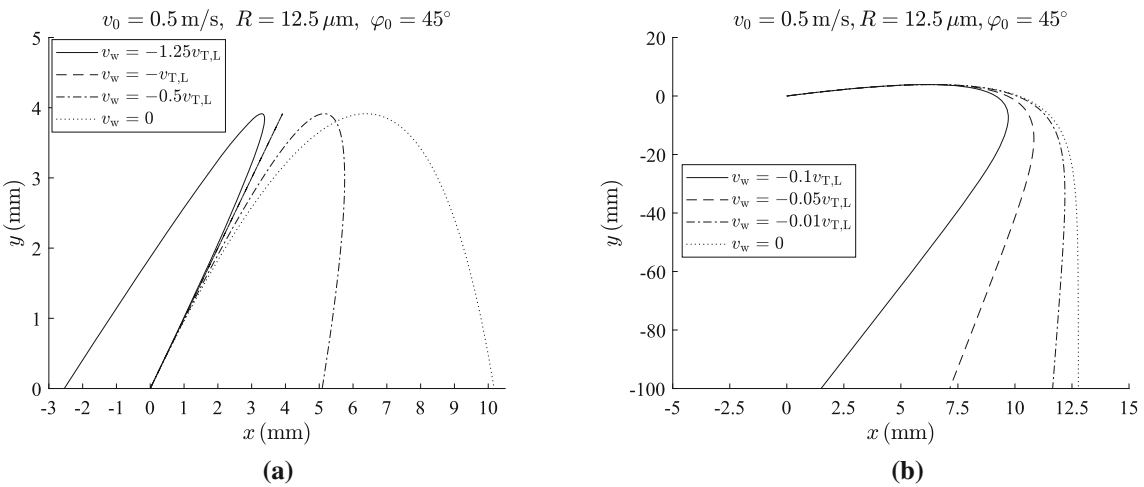

Fig. 7 **a** Early portion of the trajectory of a tungsten powder particle of diameter 25 μm ejected at $\varphi_0 = 45°$ with initial velocity $v_0 = 0.5$ m/s against a horizontal air stream with different velocity v_{w}, according to the linear drag model. For $v_{\mathrm{w}} = -v_{\mathrm{T,L}}$ the particle moves along the straight line $y = x$. For $|v_{\mathrm{w}}| > v_{\mathrm{T,L}}$, there is an upward reversal and for $|v_{\mathrm{w}}| < v_{\mathrm{T,L}}$ a downward reversal of the direction of motion. **b** Trajectories in the case of several smaller values of the backward air stream during the first 0.5 s. The ejection angle is $\varphi_0 = 45°$

moves along the straight line $y = x$. For $|v_w| > v_{T,L}$, there is an upward reversal and for $|v_w| < v_{T,L}$ a downward reversal of the direction of motion. The initial Reynolds number is 0.825 and remains less than 1 throughout the motion, validating the use of the linear drag model. Because k_L is large, the trajectories quickly approach the straight lines with the slope $-(v_{T,L}/v_w)$. In the absence of wind, the vertical asymptote of the trajectory is $x_m = (v_0/k_L)\cos(\varphi_0) = 12.8$ mm, which follows from (3.4). The trajectories in the case of several smaller values of the backward wind, all giving rise to downward reversal of the direction of motion during the first 0.5 s, are shown in Fig. 7b. The ejection angle is $\varphi_0 = 45°$. In the absence of drag, $x(y = 0) = (v_0^2/g)\sin 2\varphi_0 = 25.5$ mm, which is almost twice as large as $x_m = 12.8$ mm. The study of the projectile motion of a powder particle which includes its repeated rebounds after impacts with a flat surface has been useful in the theoretical and experimental analysis of collisions in mechanical milling processes of powder technology [52].

4 Projectile motion under nonquadratic drag

The motion of some spherical projectiles takes place in the range of the Reynolds number $1 < \mathrm{Re} < 1000$, in which neither linear nor quadratic drag model applies, but a more involved nonlinear model. Furthermore, for some projectiles the values of the Reynolds number can change during motion in such a way that during one phase of motion a quadratic drag applies, while during another phase of motion a nonquadratic drag applies. Since the extent of different phases of motion is not known in advance, it is necessary to introduce the expression for the drag force that encompasses the entire range of the Reynolds number. This is commonly done by defining the drag force as

$$\mathbf{F}_d = -\frac{1}{2}\, c_d \rho_{air} A |\boldsymbol{v} - \boldsymbol{v}_w|(\boldsymbol{v} - \boldsymbol{v}_w), \quad A = \pi R^2, \tag{4.1}$$

where the drag coefficient c_d depends on the Reynolds number according to experimental data. The following expression, adapted from [16], fits the data for a smooth spherical projectile sufficiently well in the range $0 < \mathrm{Re} \le 10^6$,

$$c_d = \begin{cases} 24\mathrm{Re}^{-1} + 3.085\mathrm{Re}^{-0.28}, & 0 < \mathrm{Re} \le 10^3, \\ 0.47, & 10^3 \le \mathrm{Re} \le 3 \times 10^5, \\ 0.1, & 3 \times 10^5 < \mathrm{Re} \le 10^6. \end{cases} \tag{4.2}$$

Below $\mathrm{Re} \approx 0.2$, the dominant contribution to c_d in (4.2) comes from the term $24/\mathrm{Re}$, which gives rise to linear drag force. To simplify the analysis, the value $c_d = 0.1$ is taken above $\mathrm{Re} = 3 \times 10^5$ as an approximate average value in the range $3 \times 10^5 < \mathrm{Re} \le 10^6$, replacing the actual nonlinear dependence of c_d on Re in that high range of the Reynolds number (characterized by partially turbulent boundary layer in the nonseparated portion of flow). In some work, the nonlinear expression for c_d is defined in the range of the Reynolds number from about 0.2 to 2×10^3. The velocity of projectile is assumed to be sufficiently below the speed of sound in air so that the dependence of the drug coefficient on the Mach number can be ignored. Recent analysis of correlations for supersonic drag coefficient of spherical particles can be found in [53,54]. The variation of c_d with Re according to (4.2) is depicted in Fig. 8a (solid curve). The experimentally determined variation is shown in Fig. 8b. The variation of the normalized drag force F_d with the Reynolds number Re, as obtained from (4.1) and (4.2), is depicted in Fig. 8a by a dash-dotted curve. While the drag coefficient is decreasing, or remains constant with the increase in the Reynolds number, the corresponding drag force is monotonically increasing, apart from a sudden drop at $\mathrm{Re} = 3 \times 10^5$ associated with a sadden drop of c_d from 0.47 to 0.1.

The differential equations of projectile motion in the case of nonlinear drag are [18]

$$\begin{aligned} \frac{dv_x}{dt} &= -\frac{1}{2}\, c_d \rho_{air}(A/m)|\boldsymbol{v} - \boldsymbol{v}_w|(v_x - v_{w,x}), \\ \frac{dv_y}{dt} &= -\frac{1}{2}\, c_d \rho_{air}(A/m)|\boldsymbol{v} - \boldsymbol{v}_w|(v_y - v_{w,y}) - g, \end{aligned} \tag{4.3}$$

with the initial conditions $v_x(0) = v_0 \cos\varphi_0$ and $v_y(0) = v_0 \sin\varphi_0$, and with c_d defined in (4.2). Equations (4.3) are two coupled nonlinear differential equations which require numerical solution, and which can be readily done by using, for example, the MATLAB function *ode45*. After the velocity components v_x and v_y have been so determined, the (x, y) coordinates of the trajectory follow by numerical quadrature from the velocity components, with the specified initial conditions for $x(0)$ and $y(0)$.

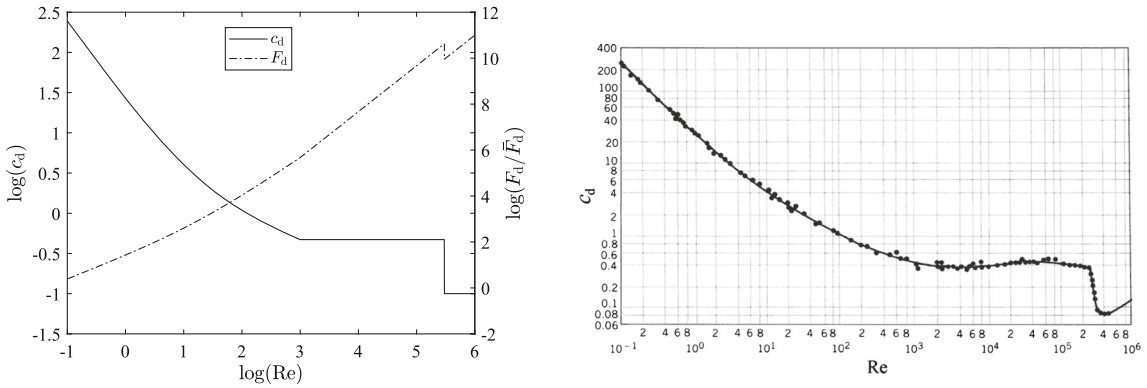

(a) **(b)**

Fig. 8 **a** Variations (on the logarithmic scale) of the normalized drag force $F_d/\bar{F}_d$ and the drag coefficient c_d with the Reynolds number according to (4.1) and (4.2). The normalizing factor is $\bar{F}_d = (\pi/8)\rho_{air}v_{air}^2$. **b** The experimentally determined variation for a smooth sphere (reproduced from [49])

Motion of a respiratory droplet

Figure 9a shows the trajectories of a respiratory droplet of radius $R = 100\,\mu$m ejected in stagnant air with initial velocity $v_0 = 10$ m/s at three different values of the angle φ_0. The evaporation of the droplet is ignored. The horizontal momentum is rapidly lost, and the vertical component of velocity rapidly approaches the value of the terminal speed (along the vertical portion of the trajectory). The corresponding variations of the Reynolds number and the drag coefficient with time are shown in Fig. 9a (in case $\varphi_0 = 45°$). Throughout the motion, the Reynolds number is in the range $5 < \mathrm{Re} < 135$, and the nonlinear expression for the drag coefficient applies $c_d = 24\mathrm{Re}^{-1} + 3.085\mathrm{Re}^{-0.28}$, as defined in (4.2). The vertical portions of the trajectories are reached as the velocity of the droplet approaches its terminal velocity (0.725 m/s). The corresponding limiting values of the Reynolds number and the drag coefficient are $\mathrm{Re} = 9.56$ and $c_d = 4.15$. The terminal velocity ($v_{T,N}$) for this nonlinear drag range is the solution of a nonlinear algebraic equation

$$v_{T,N}^{1.72} + 4.723\left(\frac{\nu_{air}}{R}\right)^{0.72} v_{T,N} - 1.05\,\frac{\rho g R}{\rho_{air}}\left(\frac{R}{\nu_{air}}\right)^{0.28} = 0, \tag{4.4}$$

which follows from the condition $F_d = mg$, where m is the mass of the droplet whose density is ρ. Figure 9b shows the trajectories of the respiratory droplet ejected with initial velocity $v_0 = 10$ m/s against the wind with velocity $|v_w| = 1$ m/s. The terminal velocity in this case is $v_{term} = (v_{T,N}^2 + v_w^2)^{1/2} = 1.235$ m/s, independently of φ_0. The evaporation of the droplet at a given relative humidity significantly affects the shape of the trajectory and increases the droplet's horizontal reach. This has been discussed in [13,55–58] in the context of the evaluation of the risks of infection by transmitted pathogenic droplets and the estimates of safe distancing during soft or loud talking and coughing. Different empirical correlations for calculating the drag coefficient in viscous spheres (liquid drops) have been listed and discussed in [59].

Motion of a flea beetle

Figure 9c shows the trajectories of a flea beetle, assumed to be of spherical shape with radius $R = 0.8$ mm and mass density 0.25 g/cm^3, corresponding to three launch angles φ_0 and the same initial velocity of 3 m/s. Only $y \geq 0$ potions of the trajectories are shown. The variations of the Reynolds number and the drag coefficient with time are shown in Fig. 10b, again in case $\varphi_0 = 45°$. Throughout the motion, the Reynolds number is in the range $120 < \mathrm{Re} < 320$. The values of the Reynolds number and the drag coefficient at the terminal velocity (2.414 m/s) are $\mathrm{Re} = 254.7$ and $c_d = 0.748$. These results are in qualitative agreement with kinematic features of the flea beetle jumps reported in [60,61]. Figure 9d shows the trajectories of the same flea beetle when it jumps against the wind with velocity $|v_w| = 2$ m/s. For $\varphi_0 = 30°$ and 45°, the downward reversal of the direction of motion takes place, while for $\varphi_0 = 60°$ the reversal of the direction of motion is upward. The terminal velocity in this case is $v_{term} = 3.135$ m/s.

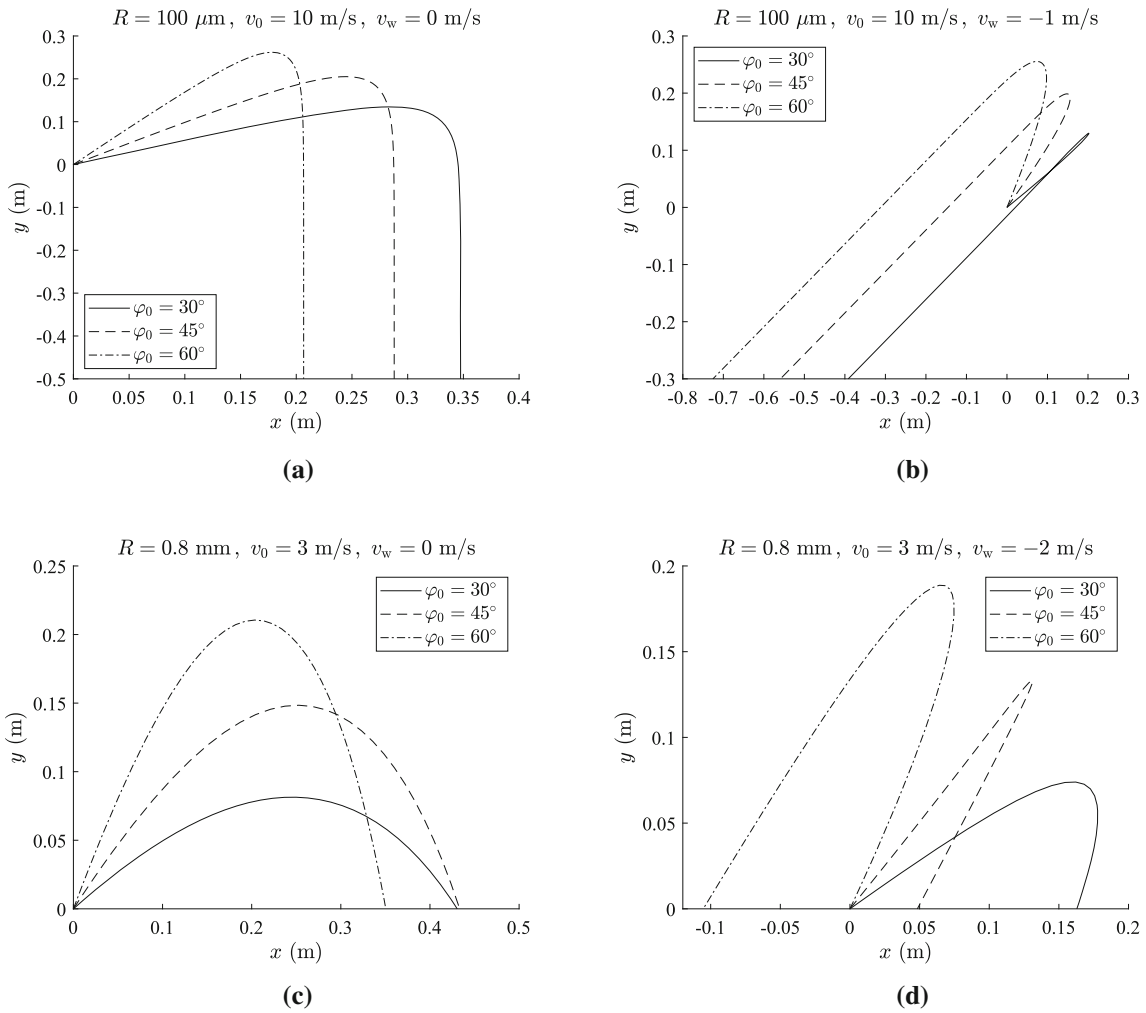

Fig. 9 **a** Trajectories of a respiratory droplet of radius $R = 100\,\mu$m ejected in stagnant air with initial velocity $v_0 = 10$ m/s at three different values of the angle φ_0. **b** Trajectories of the same respiratory droplet ejected with initial velocity $v_0 = 10$ m/s against the wind $|v_w| = 1$ m/s. **c** Trajectories of a flea beetle, assumed to be of spherical shape with radius $R = 0.8$ mm and mass density 0.25 g/cm^3, corresponding to three values of the jump angle φ_0 and the same initial velocity of 3 m/s. Only $y \geq 0$ potions of the trajectories are shown. **d** Trajectories of the flea beetle when it jumps against the wind $|v_w| = 2$ m/s

4.1 Transition from nonquadratic to quadratic drag

In all cases considered in Fig. 9, the Reynolds number throughout the motion is in the range $1 < \mathrm{Re} < 1000$, in which the same expression applies for the drag coefficient $c_d = 24\mathrm{Re}^{-1} + 3.085\mathrm{Re}^{-0.28}$, as specified by (4.2). It is not difficult to construct an example of the projectile motion in which the Reynolds number is in the range $1 < \mathrm{Re} < 10^3$ (nonquadratic drag range) during one phase of motion, and in the range $10^3 < \mathrm{Re} < 3 \times 10^5$ (quadratic drag range) during another phase of motion. For example, Fig. 11a shows the variations of the Reynolds number and the drag coefficient with time in the case of a spherical projectile of radius 2 mm and mass density 0.25 g/cm^3, launched in stagnant air with initial velocity 3 m/s at 45°. During the first 0.7 s, the Reynolds number is in the range $449 < \mathrm{Re} < 1000$, where the nonlinear expression for c_d applies, but for $t > 0.7$ s the Reynolds number is in the range $1000 < \mathrm{Re} < 1269$ (within the quadratic drag range), where the drag coefficient is constant and equal to $c_d = 0.47$. The corresponding variations of the normalized drag force $F_d/\bar{F}_d$ and the velocity v/v_0 are shown in Fig. 11b. The normalizing force is the initial value of the drag force $F_d^0 = (1/2)\rho_{air} A c_d^0 v_0^2$, where $c_d^0 = 0.506$. The terminal velocity is 4.816 m/s, which is obtained from $v_T = 2.382[(\rho/\rho_{air})gR]^{1/2}$.

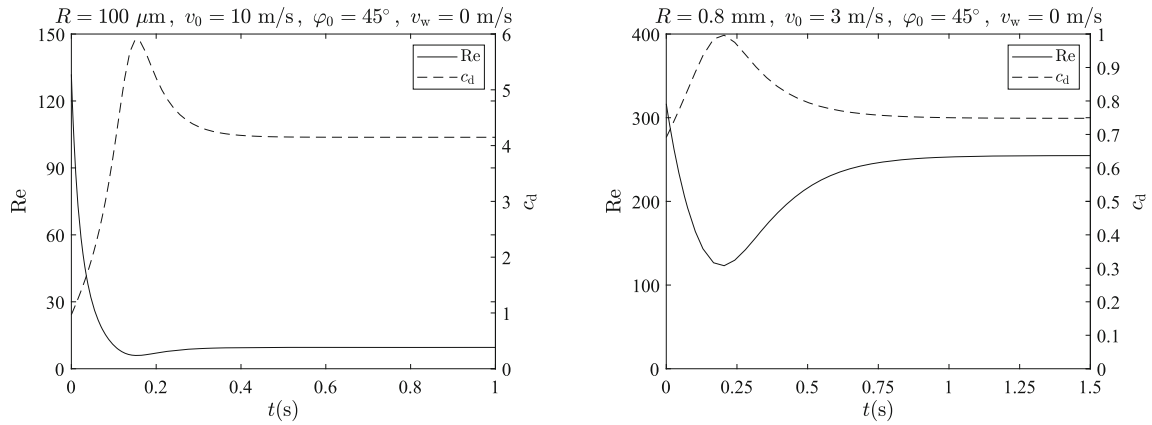

Fig. 10 **a** Variations of the Reynolds number (Re) and the drag coefficient (c_d) with time for a respiratory droplet from Fig. 9a, in case $\varphi_0 = 45°$. The Reynolds number during the motion is in the range $5 < \text{Re} < 135$. **b** Variations of the Reynolds number and the drag coefficient with time for a flea beetle from Fig. 9c, in case $\varphi_0 = 45°$. The Reynolds number during the motion is in the range $120 < \text{Re} < 320$

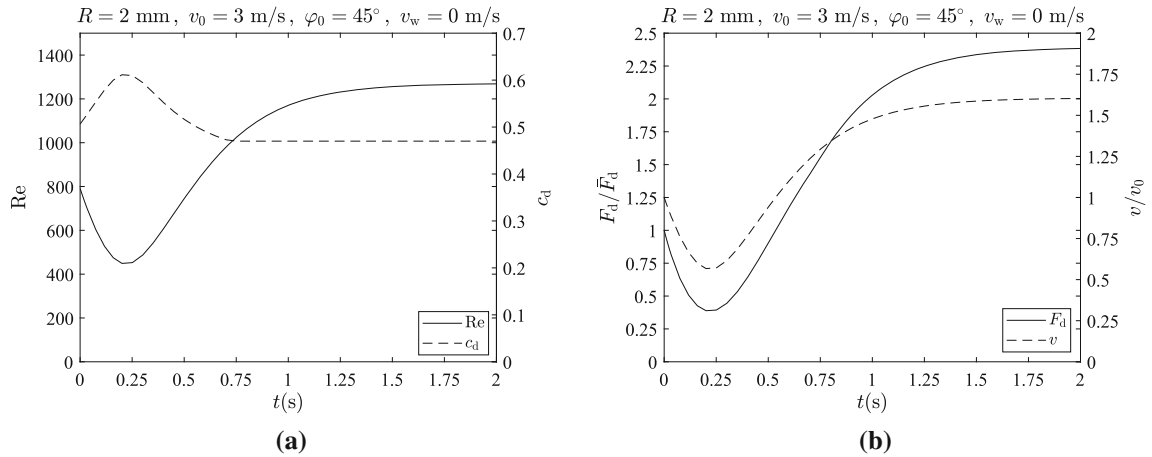

Fig. 11 **a** Variations of the Reynolds number and the drag coefficient with time in the case of a spherical projectile of radius 2 mm and mass density 0.25 g/cm^3, launched in stagnant air with initial velocity 3 m/s at 45°. During the first 0.7 s, the Reynolds number is in the range $449 < \text{Re} < 1000$, where the nonlinear expression for c_d applies, but for $t > 0.7$ s the Reynolds number is within the quadratic drag range $1000 < \text{Re} < 1269$, where the drag coefficient is constant and equal to $c_\text{d} = 0.47$. **b** The corresponding variations of the normalized drag force F_d and the normalized velocity v

4.2 Transition from quadratic drag with $c_\text{d} = 0.47$ to quadratic drag with $c_\text{d} = 0.1$

To further illustrate the pronounced effect of the value of the drag coefficient used in the expression for the drag force on the shape of the trajectory and the flight velocity of the projectile, consider a spherical projectile of mass $m = 45$ g and radius $R = 45$ mm. If the projectile is launched with initial velocity $v_0 = 40$ m/s at 30°, the Reynolds number during its motion is in the range $6.64 \times 10^4 < \text{Re} < 2.37 \times 10^5$ (in the absence of wind), and the quadratic drag applies throughout the motion, with the drag coefficient $c_\text{d} = 0.47$. However, if the projectile is launched with initial velocity $v_0 = 80$ m/s, the Reynolds number during the first 0.76 s is greater than 3×10^5, and the quadratic drag model with the drag coefficient $c_\text{d} = 0.1$ applies during that stage of motion, as specified by (4.2). Thereafter, the Reynolds number falls below the threshold value of 3×10^5, and the projectile enters the quadratic drag regime with the drag coefficient $c_\text{d} = 0.47$ (Fig. 12a). Figure 12b shows the corresponding variations of the normalized drag force and the normalized velocity during the first 6 s. The normalizing force is $\bar{F}_\text{d} = (1/2)\rho_\text{air}(\pi R^2)v_0^2$. Details of the kinematic and the kinetic analysis of the transition between different types of drag have not been previously elaborated upon, and it may be of interest to pursue this analysis further by using different correlations for the drag coefficient [16,17,59].

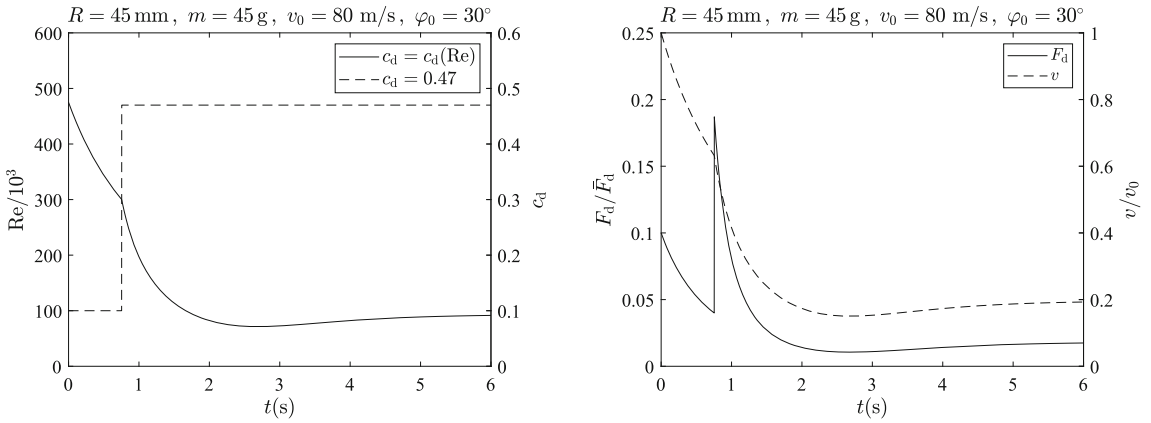

Fig. 12 Projectile motion of a spherical ball of mass $m = 45$ g and radius $R = 45$ mm launched in stagnant air with initial velocity $v_0 = 80$ m/s at $\varphi_0 = 45°$. **a** The variations of the Reynolds number and the drag coefficient with time. During the first 0.76 s, Re $> 3 \times 10^5$ and the drag coefficient is $c_d = 0.1$. Thereafter, the Reynolds number falls below the threshold value of 3×10^5, and the ball enters the quadratic drag regime with the drag coefficient $c_d = 0.47$. **b** Corresponding normalized drag force and the normalized velocity of the ball versus the time

4.3 Reaching a projectile target

To illustrate the application of the presented analysis, suppose that the objective is to determine the initial velocity v_0 required to reach a target located at the point $(x, y) = (50, 0)$ m, when the projectile motion takes place in still air, and when it takes place in the presence of horizontal wind with velocity $v_w = \pm 10$ m/s. The launch angle is $\varphi_0 = 30°$. Let the projectile be a spherical ball of mass $m = 45$ g and radius $R = 45$ mm. Figure 13 depicts the results: shown in part (a) are the trajectories, and in part (b) the velocities of the ball. In still air, the required initial velocity is $v_0 = 54$ m/s; in the presence of forward wind $v_w = 10$ m/s it is $v_0 = 33.2$ m/s, while in the presence of backward wind $v_w = -10$ m/s, it is $v_0 = 72.7$ m/s. The vertical asymptote of the trajectory in still air is $x_m = 59.32$ m, and thus the solid curve for the velocity v in still air ends in Fig. 13b at that point. In the case of backward wind, the ball reaches the maximum horizontal distance of 57 m, before reversing the horizontal direction of its motion and reaching a target point with coordinates (50, 0) m. The terminal velocity in stagnant air is 15.69 m/s, while in the presence of both forward and backward

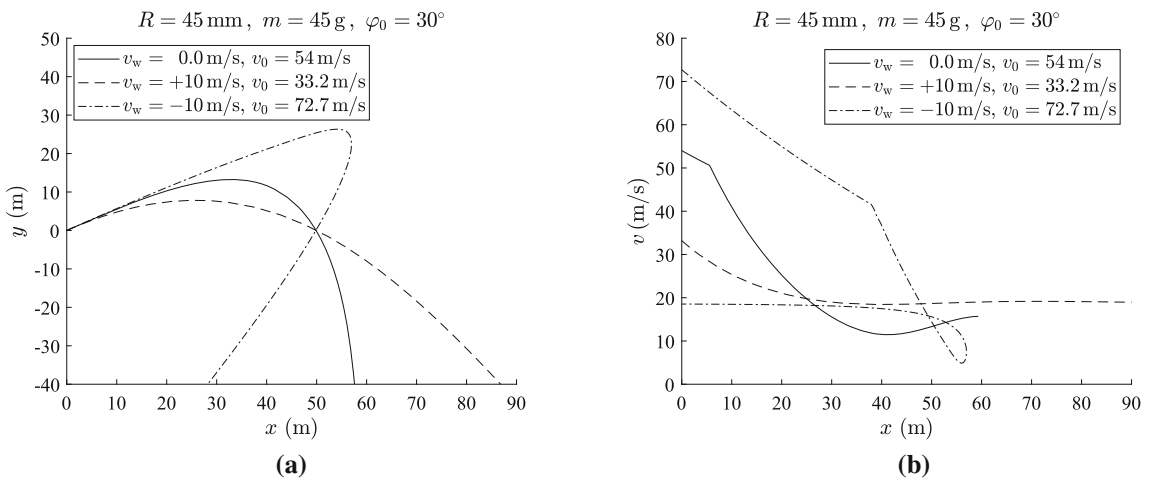

Fig. 13 **a** Trajectories of a spherical ball of mass $m = 45$ g and radius $R = 45$ mm launched at $\varphi_0 = 30°$ with the initial velocity adjusted to reach the target point $(x, y) = (50, 0)$ m. The projectile motion is taking place in either stagnant air ($v_w = 0$ m/s), or in the presence of forward or backward wind ($v_w = \pm 10$ m/s). The portions of the trajectories for $y \geq -40$ m are shown only. **b** Corresponding velocity variations

wind ($v_w = \pm 10$ m/s), the terminal velocity is $(15.69^2 + 10^2)^{1/2} = 18.61$ m/s. The drag coefficient in the case of forward wind is $c_d = 0.1$ throughout the projectile motion, while in the case of backward wind and in the case of stagnant air, the drag coefficient is initially equal to 0.1, and when the Reynolds number falls below 3×10^5 it jumps to 0.47. These results can be accordingly modified by the incorporation of the effect of the roughness of the ball and the Magnus effect due to the imparted spin to the ball and the corresponding aerodynamic force orthogonal to the velocity vector, which is of particular interest for the motion of sports balls [24–27,62,63], but which is beyond the scope of the present review. One can also perform an optimization analysis to determine the launch angle which minimizes the launch velocity required to reach a given target. In the absence of wind and with a quadratic drag model, the results of such analysis have been reported in [64].

5 Conclusion

The analysis of wind-influenced projectile motion of a spherical projectile in the presence of linear and nonlinear drag force has been reviewed. The models of ambient drag are first considered in which the drag force is either quadratic or linear in velocity. In the presence of quadratic drag, the governing differential equations are coupled and require numerical solution. The results in Sect. 2 are conveniently expressed for any value of the damping parameter c, and the specified initial velocity v_0 and the launch angle φ_0, by normalizing the spatial coordinates x and y with the length scale k^{-1}, where $k = c/m$ and m is the mass of the projectile. For projectiles launched at low angle, there is an approximate but sufficiently accurate closed-form solution. The relationship between the velocity of the projectile v and an appropriately introduced angle parameter ϕ is derived in closed-form, with or without the presence of uniform wind. The effects of wind on the trajectory and flight velocity are evaluated and discussed. The differential equations of motion in the case of linear drag, considered in Sect. 3, are decoupled and allow for an entirely closed-form solution for the velocity components and the trajectory profile. The damping coefficient in this case is denoted by c_L, while the parameter $k_L = c_L/m$ has the dimension time^{-1}. The values of k_L are commonly so large that the trajectories of the projectiles in the linear damping range (Re$<$ 1) dominantly consist of two nearly straight lines, on the time scale of a fraction of 1 s or longer. This is illustrated by the motion of a small respiratory droplet and a tungsten powder particle. Forward-to-backward transition of motion in the case of a projectile launched against horizontal wind is analyzed. The projectile motion in the range of the Reynolds number when neither linear nor quadratic drag model applies is considered in Sect. 4. If projectile motion consists of phases with different types of drag, the extents of which are not known in advance, the general expression for the drag force, which encompasses the entire range of the Reynolds number, must be used throughout the motion, in conjunction with the numerical solution of the governing nonlinear differential equations of motion. Transition from nonquadratic to quadratic drag is then discussed. Illustrative examples considered in this review include projectile motions of golf balls, respiratory droplets, powder particles, and flea beetles. In addition to being of research and technological interest, the presented analysis and results are appealing from the pedagogical point of view and for the incorporation in undergraduate research projects, which can be beneficial to the scholarly and professional development of engineering students [65,66].

Acknowledgements Valuable comments and suggestions by anonymous reviewers are gratefully acknowledged.

Declarations

Conflict of interest On behalf of all authors, the corresponding author states that there is no conflict of interest.

References

1. Timoshenko, S., Young, D.: Advanced Dynamics. McGraw-Hill, New York (1948)
2. Long, L.N., Weiss, H.: The velocity dependence of aerodynamic drag: a primer for mathematicians. Am. Math. Mon. **106**, 127–135 (1999). https://doi.org/10.1080/00029890.1999.12005019
3. Timmerman, P., Van der Weele, K.: On the rise and fall of a ball with linear or quadratic drag Am. J. Phys. **67**, 538–546 (1999). https://doi.org/10.1119/1.19320
4. Fay, T.H.: Quadratic damping. Int. J. Math. Educ. Sci. Technol. **43**, 789–803 (2012). https://doi.org/10.1080/0020739X.2011.622806
5. Charbonnier, P.: Traité de Balistique Extérieure. Librairie Polytechnique, Paris (1904)

6. Symon, K.R.: Mechanics, 2nd edn. Addison-Wesley, Reading (1960)
7. De Mestre, N.: The Mathematics of Projectiles in Sport. Cambridge University Press, New York (1990)
8. White, C.: Projectile Dynamics in Sport: Principles and Applications. Routledge, London (2010)
9. Groetsch, C.W., Cipra, B.: Halley's comment: projectiles with linear resistance. Math. Mag. **70**, 273–280 (1997)
10. Morales, D.A.: Exact expressions for the range and the optimal angle of a projectile with linear drag. Can. J. Phys. **83**, 67–83 (2005). https://doi.org/10.1139/p04-072
11. Purcell, E.M.: Life at low Reynolds number. Am. J. Phys. **45**, 3–11 (1977). https://doi.org/10.1119/1.10903
12. Aguirre-López, M.A., Almaguer, F.J., Díaz-Hernández, O., Escalera Santos, G.J., Javier Morales-Castillo, J.: On continuous inkjet systems: a printer driver for expiry date labels on cylindrical surfaces. Adv. Comput. Math. **45**, 2019–2028 (2019). https://doi.org/10.1007/s10444-019-09682-0
13. Lubarda, M.V., Lubarda, V.A.: On the motion of an evaporating respiratory droplet. Proc. Monten. Acad. Sci. Arts **25** (2022) (**in press**). arXiv:2105.09066 [physics.app-ph]
14. White, F.M.: Viscous Fluid Flow, 3rd edn. McGraw-Hill, New York (2006)
15. Cohen, C., Darbois-Texier, B., Dupeux, G., Brunel, E., Quéré, D., Clanet, C.: The aerodynamic wall. Proc. R. Soc. Lond. A **470**, 20130497 (2014). https://doi.org/10.1098/rspa.2013.0497
16. Khan, A.R., Richardson, J.F.: The resistance to motion of a solid sphere in a fluid. Chem. Eng. Commun. **62**(1–6), 135–150 (1987). https://doi.org/10.1080/00986448708912056
17. Polezhaev, Y.V., Chircov, I.V.: Drag coefficient. Thermopedia (2020). https://doi.org/10.1615/AtoZ.d.drag_coefficient
18. Ray, S., Fröhlich, J.: An analytic solution to the equations of the motion of a point mass with quadratic resistance and generalizations. Arch. Appl. Mech. **85**, 395–414 (2015). https://doi.org/10.1007/s00419-014-0919-x
19. Parker, G.W.: Projectile motion with air resistance quadratic in the speed. Am. J. Phys. **45**, 606–610 (1977). https://doi.org/10.1119/1.10812
20. Warburton, R.D.H., Wang, J., Burgdörfer, J.: Analytic approximations of projectile motion with quadratic air resistance. J. Serv. Sci. Manag. **3**, 98–105 (2010). https://doi.org/10.4236/jssm.2010.31012
21. Chudinov, P.S.: The motion of a point mass in a medium with a square law of drag. J. Appl. Math. Mech. **65**, 421–426 (2001). https://doi.org/10.1016/S0021-8928(01)00047-8
22. Chudinov, P.S.: Analytical investigation of point mass motion in midair. Eur. J. Phys. **25**, 73–79 (2004). https://doi.org/10.1088/0143-0807/25/1/010
23. Turkyilmazoglu, M.: Highly accurate analytic formulae for projectile motion subjected to quadratic drag. Eur. J. Phys. **37**, 035001 (2016). https://doi.org/10.1088/0143-0807/37/3/035001
24. Nathan, A.M.: The effect of spin on the flight of a baseball. Am. J. Phys. **76**, 119–124 (2008). https://doi.org/10.1119/1.2805242
25. Robinson, G., Robinson, I.: The motion of an arbitrarily rotating spherical projectile and its application to ball games. Phys. Scr. **88**, 018101 (2013). https://doi.org/10.1088/0031-8949/88/01/018101
26. Turkyilmazoglu, M., Altundag, T.: Exact and approximate solutions to projectile motion in air incorporating Magnus effect. Eur. Phys. J. Plus **135**, 566 (2020). https://doi.org/10.1140/epjp/s13360-020-00593-4
27. Cross, R.: Vertical bounce of a spinning ball. Phys. Educ. **56**, 023002 (2021). https://doi.org/10.1088/1361-6552/abd0d8
28. Bernardo, R.C., Esguerra, J.P., Vallejos, J.D., Canda, J.J.: Wind-influenced projectile motion. Eur. J. Phys. **36**, 025016 (2015). https://doi.org/10.1088/0143-0807/36/2/025016
29. Ozarslan, R., Bas, E., Baleanu, D., Acay, B.: Fractional physical problems including wind-influenced projectile motion with Mittag-Leffler kernel. AIMS Math. **5**, 467–481 (2020). https://doi.org/10.3934/math.2020031
30. Vogel, S.: Living in a physical world II. The bio-ballistics of small projectiles. J. Biosci. **30**, 167–175 (2005). https://doi.org/10.1007/BF02703696
31. Vogel, S.: The bioballistics of small projectiles. In: Glimpses of Creatures in Their Physical Worlds, pp. 18–38. Princeton University Press, Princeton. https://doi.org/10.1515/9781400833863.18
32. Warburton, R.D.H., Wang, J.: Analysis of asymptotic projectile motion with air resistance using the Lambert function. Am. J. Phys. **72**, 1404–1407 (2004). https://doi.org/10.1119/1.1767104
33. Stewart, S.M.: An analytic approach to projectile motion in a linear resisting medium. Int. J. Math. Educ. Sci. Technol. **37**, 411–431 (2006). https://doi.org/10.1080/00207390600594911
34. Hu, H., Zhao, Y.P., Guo, Y.J., Zheng, M.Y.: Analysis of linear resisted projectile motion using the Lambert W function. Acta Mech. **223**, 441–447 (2012). https://doi.org/10.1007/s00707-011-0571-2
35. Benacka, J.: Simulating projectile motion in the air with spreadsheet. Spreadsheets Educ. (eJSiE) **3**, 1–7 (2009)
36. Grigore, I., Miron, C., Barna, E.S.: Exploring excel spreadsheets to simulate the projectile motion in the gravitational field. Rom. Rep. Phys. **69**, 1–14 (2017)
37. Hackborn, W.W.: Projectile motion: resistance is fertile. Am. Math. Mon. **115**, 813–819 (2008)
38. Hackborn, W.W.: On motion in a resisting medium: a historical perspective. Am. J. Phys. **84**, 127–134 (2016). https://doi.org/10.1119/1.4935896
39. Watts, R.G., Ferrer, R.: The lateral force on a spinning sphere: aerodynamics of a curveball. Am. J. Phys. **55**, 40–44 (1987). https://doi.org/10.1119/1.14969
40. Smith, L., Sciacchitano, A.: Baseball drag measurements in free flight. Appl. Sci. **12**, 1416 (2022). https://doi.org/10.3390/app12031416
41. Allen, E.J.: Approximate ballistics formulas for spherical pellets in free flight. Def. Technol. **14**, 1–11 (2018). https://doi.org/10.1016/j.dt.2017.11.004
42. Taylor, J.R.: Classical Mechanics. University Science Books, Sausalito (2005)
43. Thornton, S.T., Marion, J.B.: Classical Dynamics of Particles and Systems, 5th edn. Brooks Cole, Belmont (2003)
44. Fowles, G., Cassiday, G.L.: Analytical Mechanics, 7th edn. Thomson Brooks/Cole, Belmont (2005)
45. Lubarda, M.V., Lubarda, V.A.: Inelastic bouncing of a spherical ball in the presence of quadratic drag with application to sports balls. Proc. IMechE Part P J. Sports Eng. Technol. (2022) (**in press**)

46. Lubarda, M.V., Lubarda, V.A.: An analysis of pendulum motion in the presence of quadratic and linear drag. Eur. J. Phys. **42**, 055014 (2021). https://doi.org/10.1088/1361-6404/ac1446
47. Hayen, J.C.: Projectile motion in a resistant medium. Part I: Exact solution and properties. Int. J. Nonlinear Mech. **38**, 357–369 (2003). https://doi.org/10.1016/S0020-7462(01)00067-1
48. Rooney, F.J., Eberhard, S.K.: On the ascent and descent times of a projectile in a resistant medium. Int. J. Nonlinear Mech. **46**, 742–744 (2011). https://doi.org/10.1016/j.ijnonlinmec.2011.02.007
49. Munson, B.R., Young, D.F., Okiishi, T.H.: Fundamentals of Fluid Mechanics. Wiley, New York (1990)
50. Corless, R.M., Gonnet, G.H., Hare, D.E.G., Jeffrey, D.J., Knuth, D.E.: On the Lambert W function. Adv. Comput. Math. **5**, 329–359 (1996). https://doi.org/10.1007/BF02124750
51. Hu, H., Guo, Y.J., Xu, D.Q.: Relationship between the elastic-plastic interface radius and internal pressure of thick-walled cylinders using the Lambert W function. Arch. Appl. Mech. **83**, 643–646 (2013). https://doi.org/10.1007/s00419-012-0699-0
52. Suzuki, A., Maruoka, N., Oishi, Y., Kawai, H., Nogami, H.: Simulation of powder motion with particle contact model including intervening liquid. ISIJ Int. **60**, 1538–1544 (2020). https://doi.org/10.2355/isijinternational.ISIJINT-2020-072
53. Loth, E., Daspit, J.T., Jeong, M., Nagata, T., Nonomura, T.: Supersonic and hypersonic drag coefficients for a sphere. AIAA J. **59**, 3261–3274 (2021). https://doi.org/10.2514/1.J060153
54. Singh, N., Kroells, M., Li, C., Ching, E., Ihme, M., Hogan, C.J., Schwartzentruber, T.E.: General drag coefficient for flow over spherical particles. AIAA J. **60**, 587–597 (2022). https://doi.org/10.2514/1.J060648
55. Liu, L., Wei, J., Li, Y., Ooi, A.: Evaporation and dispersion of respiratory droplets from coughing. Indoor Air **27**, 179–190 (2017). https://doi.org/10.1111/ina.12297
56. Cheng, C.H., Chow, C.L., Chow, W.K.: Trajectories of large respiratory droplets in indoor environment: a simplified approach. Build. Environ. **183**, 107196 (2020). https://doi.org/10.1016/j.buildenv.2020.107196
57. Wang, H., Li, Z., Zhang, X., Zhu, L., Liu, Y., Wang, S.: The motion of respiratory droplets produced by coughing. Phys. Fluids **32**, 125102 (2020). https://doi.org/10.1063/5.0033849
58. Lieber, C., Melekidis, S., Koch, R., Bauer, H.J.: Insights into the evaporation characteristics of saliva droplets and aerosols: levitation experiments and numerical modeling. J. Aerosol Sci. (2021). https://doi.org/10.1016/j.jaerosci.2021.105760
59. Wegener, M., Paul, N., Kraume, M.: Fluid dynamics and mass transfer at single droplets in liquid/liquid systems. Int. J. Heat Mass Transf. **71**, 475–495 (2014). https://doi.org/10.1016/j.ijheatmasstransfer.2013.12.024
60. Brackenbury, J., Wang, R.: Ballistics and visual targeting in flea-beetles (Alticinae). J. Exp. Biol. **198**, 1931–1942 (1995). https://doi.org/10.1242/jeb.198.9.1931
61. Nadein, K., Betz, O.: Jumping mechanisms and performance in beetles. I. Flea beetles (Coleoptera: Chrysomelidae: Alticini). J. Exp. Biol. **219**, 2015–2027 (2016). https://doi.org/10.1242/jeb.140533
62. Smits, A.J., Ogg, S.: Aerodynamics of the golf ball. In: Hung, G.K., Pallis, J.M. (eds.) Biomedical Engineering Principles in Sports. Bioengineering, Mechanics, and Materials: Principles and Applications in Sports, vol. 1. Springer, Boston (2004)
63. Escalera Santos, G.J., Aguirre-López, M.A., Díaz-Hernández, O., Hueyot-Zahuantitla, F., Morales-Castillo, J., Almaguer, F.-J.: On the aerodynamic forces on a baseball, with applications. Front. Appl. Math. Stat. **4**, 66 (2019). https://doi.org/10.3389/fams.2018.00066
64. Chudinov, P.S.: An optimal angle of launching a point mass in a medium with quadratic drag force, pp. 1–8. arXiv:physics/0506201 [physics.class-ph] (2005)
65. Linn, M.C., Palmer, E., Baranger, A., Gerard, E., Stone, E.: Undergraduate research experiences: impacts and opportunities. Science **347**(6222), 1261757 (2015). https://doi.org/10.1126/science.1261757
66. Parker, J.: Undergraduate research, learning gain and equity: the impact of final year research projects. High. Educ. Pedagog. **3**, 145–157 (2018). https://doi.org/10.1080/23752696.2018.1425097